Politecnico di Torino

Degree program in Energy and Nuclear engineering

A.A. 2025/2026

March 31st, 2026

Master's Thesis

Enhancing the Value Proposition of Large-Scale Thermal Energy Storage Through Data-Driven Analysis

Written in collaboration with Technical University of Denmark

Author:

Mattia Semeraro

Supervisors:

Adriano Sciacovelli, Elisa Guelpa

Politecnico di Torino

Table of contents

List of Figures

List of Tables

Abstract

The decarbonization of heavy industries is one important challenge of our time, due to the wide usage of non-sustainable fuels. The electrification of the high temperature processes is a valuable path, but it is subject to the high volatility of the electricity prices. This thesis aims to reduce the effect of this volatility operating on the intermittent purchase of electricity and the storage of the produced heat in a sensible packed beds thermal energy storage PBTES. The focus of the first part of the thesis is modelling of a 1D 2 phase model of the storage based on the heat equation, and the analysis of the storage properties, materials and size in order to make it suitable for the dynamic operation. The second part aims to implement an algorithm to control the electricity purchase and then make an economic evaluation of the investment thought a data-based analysis. Based on 8 years (2015-2023) electricity and gas prices in Denmark, the operation of the PBTES has satisfied the temperature constraint of the user for over 98% of the time and the investment in this system 22% higher than a reference gas burner. Further development of this topic can be through new purchase algorithms, the relocation of the study in different countries or the study of local bigger or diversified renewable power plants integration.

Introduction

The world population has been trying to store energy in many forms since ancient times, the universe itself is an inexorable flux of energy, no human knows how this started, and I am confident that it will not stop soon. The first uses of energy storage have been for defence uses, villages built on hills made easy for the inhabitants to throw stones and logs to the invaders at the bottom of the hill, storing their potential energy until the moment they needed to convert it in kinetic energy [1]. Today energy is manipulated every day in different forms, and its storage is a crucial aspect of the scientific research.

Heat is essential for everyone's life, and its storage has been a challenge for many years. But what is it? The comparison I made many times to explain what a thermal energy storage is, when talking to outsiders, is the coffee thermos, well known by everyone and essential for us students, an item where you can store heated media (precious freshly brewed coffee), keep it in its high energy state for long time, and be able to use it when it is more needed. The thermal energy storage TES deals with the same problem but with a different scale, we need to store high temperature thermal energy for long time, with the least possible losses, but in a much bigger capacity than a thermos, for an amount of time that depends on the application and can go from some hours to many months.

Thermal energy storage is becoming essential for our lives, the deregulated energy markets, the non-predictable fluctuation of energy production by the renewable energy plants, the increase of the industrial and domestic heat need are some of the many issues that provide good reason for the development of thermal energy storages, that can act as a barrier to the waste of energy and to the increasing cost of energy. In reference [2] several types of configurations with hybrid power production systems and energy storages are analysed, revealing that the configurations with TES are the most affordable, reliable, and environmentally friendly.

Most of the other mature energy storage systems (figure 1) have limitations that makes them not suitable for many applications, due to limited size, geographical constraints (e. g. pumped hydro power), environmental impact (e.g. compressed air energy storage), cost and short lifecycle [3] .

The Packed Beds Sensible Thermal Energy Storage (PBTES from now on), being part of the TES family is indeed affordable and environmentally friendly, thanks to the wide availability of the materials and simple geometry of the tank; reliable, because of the low safety risks, easy maintenance; efficient, in fact a properly insulated PBTES has a round

trip efficiency over 90% for mid-term operations (from days to few weeks) [4]. These advantages position PBTES as a promising technology to support countries undergoing deep energy transitions. Denmark, for instance, offers a relevant case study due to its highly renewable and liberalized electricity market.

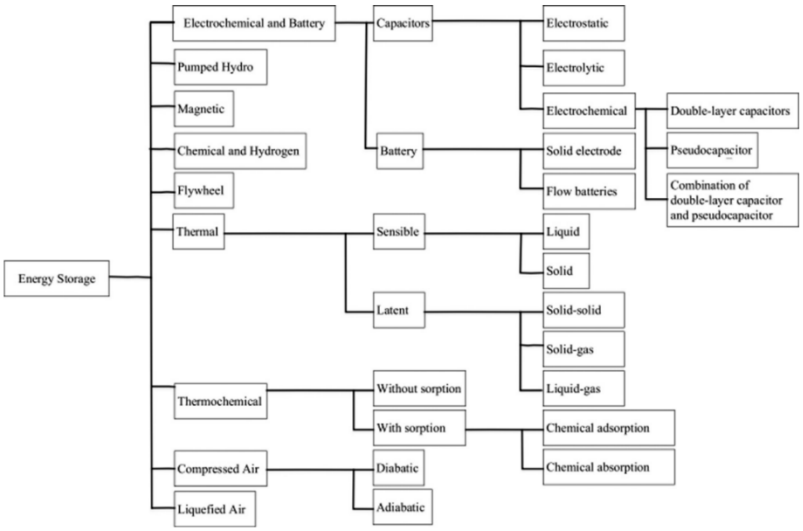

Figure 1: types of energy storage, from [5]

Denmark's electricity system represents a benchmark in Europe for renewable integration, market liberalization, and grid modernization. Since the late 1990s, Denmark has pursued a systematic liberalization of its electricity market, separating generation and retail from transmission and distribution, and enabling full consumer choice by 2003. The country maintains one of the highest shares of wind power globally, with wind energy now covering over half of its annual electricity consumption. This renewable dominance has introduced strong dynamics into the market, with wholesale electricity prices closely tied to fluctuations in wind production. When wind output is high, prices often decline sharply, even entering negative territory, while low-wind periods drive reliance on imports or thermal units, pushing prices upward [6].

This Master's Thesis builds upon this limitation, investigating the potential of a technology still at an early stage of commercialization, as the PBTES, to provide solution to the instability of the increasing renewable energy plants being constructed in most of the states to substitute fossil-based plants.

Aim of the thesis

The management of the available resources is essential to exploit the most possible energy we can. We all have the moral duty of waste the least possible resources, the many reasons of it are economic, environmental and social, everyone alive knows what I am talking about. In industrial areas this concept is even more important than in our everyday life, the magnitude of the energy used, of the losses, of the money involved is way bigger, so every further improvement can affect positively the places, people and workers around it.

The aim of this thesis is to find a way to optimize the inlet thermal energy fluxes in a PBTES, so that it can use most of the thermal power given by the available resources, and to manage the outlet flux in a way that the user can get the best gain possible from it.

Until now the TES has been treated as a passive load, storing and dispatching some industrial heat when needed, with this analysis the TES becomes an active part of the industrial area, coordinating the heat produced, consumed and giving stability to the electricity grid. This will be done through a data driven analysis inspired from the needs of an innovative industrial area GreenLab, "*a green and circular industrial park located in Skive, Denmark*"[7], a private project created in collaboration with DTU. The optimization of the system should be enough to use less grid power, produced by fossils in a relevant amount, taking advantage of the flue energy fluxes from the near industries and the renewable energy produced on site. Having an undersized transformer and distribution grid makes the construction much cheaper and maintenance faster. This is a new field in thermal energy storage (TES) field, until now they are mainly used for seasonal storage, giving low environmental gains and return on investment. The hourly/daily use of this technology can affect the society's perception on TES, opening to a new kind of use, this work will prove whether it is effective or not.

Once the optimization code is ready, it can be easily adapted to many types of data, finding the best way to use resources in many kinds of applications. A similar system and method can be applied on industrial area, districts, communities, which have different resources based on the place they are, the size and the typology of them. This can lead to interesting new results that can influence positively the planet and the people life.

Research questions

RQ1. Is the PBTES suitable for short term or dynamic behaviour?

RQ2. What strategies can be applied to maximize the benefits of a PBTES systems?

RQ3. How does the implementation of a dynamic behaviour on a PBTES improve the resilience and flexibility of the electricity and district heating grid? Is this method a valid support for the decarbonization of the hard-to-abate industrial sector?

State of the art

Summing up the previous parts this thesis is going to explore the optimization of the utilization of a PBTES in industrial applications. In the next section the PBTES technology and the Danish electricity market are going to be explored, facilitating the following reading of the thesis.

1.1. The PBTES

The main forms of heat storage are sensible, latent and thermochemical. Thermochemical heat storage is the most innovative and its development increased over the last decade; it is based on chemical reversible reactions which are endothermic and exothermic depending on specific factors. Latent heat storage exploits phase change materials which store energy in their physical state, this technology is near to the commercial but today it is being tested on a MW scale. Sensible heat storage is the most simple and mature technology; it exploits the heat contained in the high temperature of a hot media (this is the one I am going to dig in the most in this thesis).

1.1.1. PBTES as a solution

Among the different storage technologies, PBTES stands out for its favourable compromise between cost, durability, and thermodynamic performance. While electrochemical systems such as Li-ion batteries and SMES deliver high power density (up to 350 Wh/kg) and millisecond response times, their high specific costs (up to 7000 €/kWh) and limited lifespans restrict large-scale use. Mechanical systems like pumped hydro or compressed air storage reach very large capacities (hundreds to thousands of megawatts) and lifetimes exceeding 40 years, but they require specific geographic conditions and involve high infrastructure costs. Chemical storage technologies such as hydrogen or ammonia provide extremely high energy densities (up to 10 000 Wh/kg) but low efficiencies (20–50 %). In contrast, PBTES achieves round-trip efficiencies of more than 90% with minimal environmental impact and low capital cost, while maintaining excellent thermal stability over many cycles. These features make thermal energy storage systems particularly suitable for industrial waste-heat recovery and renewable integration, offering a practical bridge between high-density electrochemical devices and geographically constrained large-scale mechanical storage [8]. However, TESs also present intrinsic limitations when the stored thermal energy is intended to be reconverted into electricity. The current heat-to-electricity conversion methods, mainly based on Rankine or Brayton cycles, operate with relatively low efficiencies, typically below 60% [9], which makes PBTES unsuitable for direct electrical energy storage.

Nevertheless, PBTES offers remarkable versatility in practical applications that extend beyond direct electricity storage. When integrated with concentrating solar power (CSP)

plants, packed-bed (PB from now on) systems enable the storage of high-temperature heat collected during peak irradiation and its release during low-sunlight periods, thus improving dispatchability and plant efficiency. Several studies have shown that such configurations can reduce total system costs by up to 14 % compared with conventional two-tank molten-salt systems or other high-temperature media [10].

Beyond solar applications, the industrial heat-recovery potential of PBTES is significant (figure 2). In sectors such as steelmaking—particularly electric-arc furnaces—and ceramics manufacturing, large quantities of waste heat can be captured and stored in PB, then reused for process heating or for electricity generation through secondary cycles. This approach supports both energy efficiency and decarbonization in high-temperature industries [10].

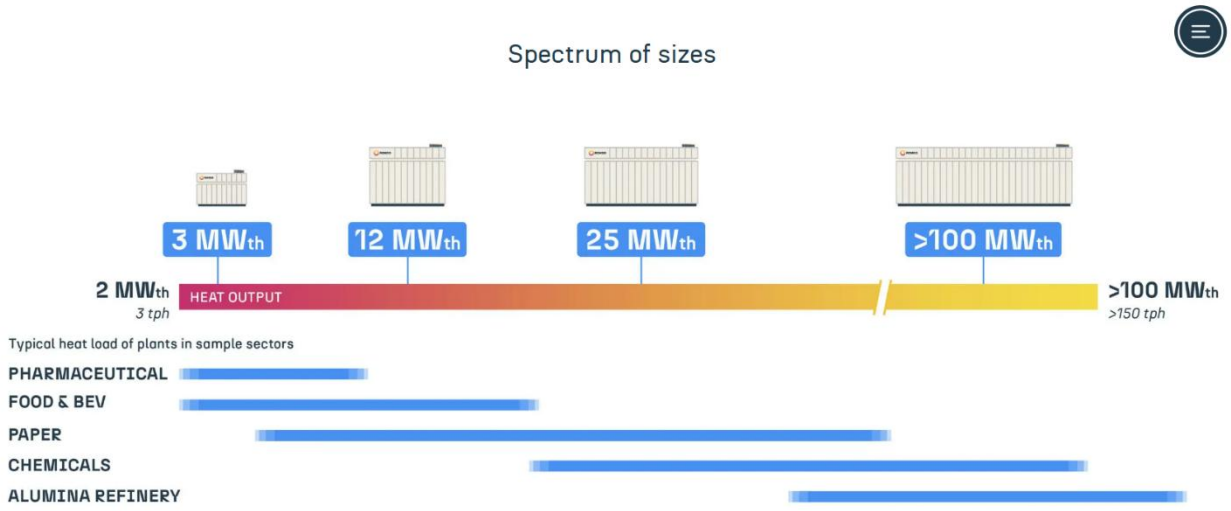

Figure 2 from Rondo.com/products [11]

Moreover, PBTES plays a growing role in power-to-heat and long-duration energy-storage concepts. In pumped-thermal electricity storage (PTES), excess electricity is converted into high-temperature heat, stored in a PB medium, and reconverted into electricity via a Brayton or Rankine cycle when needed [12]. Likewise, PBTES can be combined with compressed-air energy storage (CAES)—especially in adiabatic CAES configurations—where thermal storage mitigates efficiency losses during air compression and expansion. Numerical studies have demonstrated favourable synergies and significant efficiency gains when high-temperature PB are integrated into CAES systems [13].

In summary, although PBTES is not ideally suited for direct heat-to-power conversion, it represents a key enabling technology for renewable integration, waste-heat recovery, and hybrid storage systems, bridging the gap between electrochemical and large-scale mechanical storage.

1.1.2. Description and properties of PBTES

The PBTES is one of the most successful way to store sensible thermal energy, it is made of 2 media, usually a solid one and a fluid one, the different properties of the media, well described in the next pages, make them suitable for storing energy in a wide range of temperature, usually from 100 °C to over 1000 °C and low cost compared to the other type of systems with the same features.

Visually a PBTES can be described by a cylindric tank (figure 3 [14]), the main task of the geometry is to have its surface to volume ratio small but easy and cheap to produce and maintain, so that the heat dissipation can be low with efficiency benefits. The walls are made of insulating materials, mainly ceramic or polymeric to help this.

Figure 3 The largest industrial thermal energy storage system, at KALL Ingredients' corn processing facility in Tiszapüspöki, Hungary. From Kyoto Group website

Inside of it, it is composed by a solid media, the most common are beads, rocks, sand, but many others are examined in literature. Their aim is to have a big thermal capacity $\left(> 1000\ \frac{kJ}{m^3 K}\right)$, giving to the storage the biggest energy density, but they also must have low thermal conductivity $\left(< 5\ \frac{W}{m\ K}\right)$, so that the output flux from the media is low and can be negligible for low mass flow rates (less losses due to energy dissipation) [15]. In Table 1 (from [15]) material characteristics are displayed. Materials used are often natural rocks and pebbles, mineral product as magnetite or industrial and construction wastes. The use of wastes from other processes as solid media is also a hot research topic, due to the heterogeneity of their physical and chemical properties, each waste stream exhibits different characteristics., this makes it difficult to catalogue waste materials and to do

generalized studies with low error [16], in several cases their properties are well suited for integration into thermal energy storage systems[17].

Table 1: Solid Materials properties

Material	**Density (g/cm³)**	**Thermal Conductivity at 20 °C (W/m·K)**	**Specific Heat at 20 °C (J/kg·K)**	**Thermal Capacity (kJ/m³·K)**
Concrete	2.2–2.7	0.9–2.0	750–1130	1680–3005
HT concrete	2.8	1.0	916	2519
High-alumina	2.4	0.2	980	2352
Reinforced concrete	2.2	1.5	850	1870
Cement mortar	1.9–2.0	0.6–0.7	642	1194–1309
Castable ceramic	3.5	1.4	866	3031
Alumina ceramics	3.8–4.0	18.0–33.0	755–880	2831–3484
Silicon carbide	3.2	120.0	750	2407
Brick	1.7–1.8	0.5–0.7	840	1419–1512
Magnesia brick	3.0	5.0–5.1	1130–1150	3390–3450
Silica fire brick	1.8	1.5	1000	1820
Soil (clay)	1.5	1.3	880	1276
Soil (dry)	1.3	0.3	795	1001
Soil with gravel	2.0	0.5	1840	3680
Silica-based	2.3	1.8	863	2019
Copper	8.3–9.0	372.0–385.0	383–419	3178–3729
Cast iron	7.2–7.9	29.3–73.0	465–837	3348–6612
Aluminum	2.7	204.0–238.4	896–945	2419–2551
Cast steel	7.8	40.0–50.0	571–600	4453–4680
Steel slag	3.0	2.0–3.5	996	2968
Cofalit	3.1	1.4–2.7	800–1034	2496–3226
Graphite	2.2–2.3	122.0–155.0	401–610	882–1378
Soda-lime glass	2.7	0.9	703	1905
Sodium chloride	2.2	6.5–7.0	850–860	1836–1861
Molten salts	0.5–2.6	0.2–2.0	1500	1350–3900
Solar salt	1.9	0.5	1495	2825
Mineral oil	0.8	0.1	2600	2002
Synthetic oil	0.9	0.1	2100–2300	1890–2070
Liquid sodium	0.9	71.0	1300	1105
Water	1.0	0.6	4187	4174

Recent studies have also addressed the environmental impact of PBTES through life cycle assessment (LCA). *Nahhas et al. (2020)* [18] analysed an air–rock PB using basalt and air as heat transfer fluid, showing that the system can achieve 65 % lower cumulative energy demand, 60 % lower global warming potential, and 80 % lower water consumption compared with molten-salt tanks. The total life-cycle indicators were only $0.024 \frac{MJ_{eq}}{kWh}$, $1.5 \frac{gco_{2,eq}}{kWh}$, and $0.02 \frac{L_{eq}}{kWh}$ with both energy and carbon payback times of around two months over a 25-year lifespan, demonstrating the sustainability of natural-rock fillers as low-

impact materials . Similarly, Oró et al. (2014) [19] compared solid-media concrete storage with molten-salt systems and found that the solid option has an environmental impact of about $0.15\ \frac{EI99\ points}{kWh}$, nearly two orders of magnitude lower than molten-salt storage $\left(\approx 5.7\ \frac{EI99\ points}{kWh}\right)$, mainly because over 94 % of the molten-salt impact derives from nitrate production. These LCAs confirm that PBTES or solid-media TES not only use abundant, low-cost fillers but also represent environmentally preferable solutions for large-scale thermal energy storage.

The gaseous or liquid media is called high temperature fluid HTF. Its role is to move the heat in and out of the PBTES, flowing among the solid media. This can be made by a variety of materials according with the application of the PBTES. The most popular are air, water, molten salts and thermal oils (e.g. Therminol VP-1© and Therminol 66©), depending on the performance needed, the work temperature and of course economic evaluations [16]. M. Cascetta et al. [20] analyzed the behivour of air, water and molten salt as HTF.

The efficiency of the system in long-term applications decreases mainly for two factors: the geometry and the insulation of the tank and the thermocline degradation. Regarding the first aspect, PBTES are typically designed in cylindrical or truncated pyramid geometry, these configurations minimize the surface to volume ratio (which implies a lower heat dissipation), while ensuring adequate mechanical resilience. Moreover, the thermal insulation is designed to come close to adiabatic conditions over short time periods; however, in long-term operation, heat losses become unavoidable, leading to a progressive decrease in stored energy.

The second factor is related to the thermocline behavior, the temperature inside the PBTES is optimized in order to have the maximum exergy in the system, with a region, called thermocline, in which the majority of the temperature gradient is, dividing the hot and the cold region and keeping the temperatures almost constant in the remaining part of the storage, the exergy of the system is higher the thinner is this region. During the standby of the system the phenomena called thermocline degradation appears: the thermal conductivity of the solid, the fluid mixing and the non-uniformity of the medias amplifies the thickness of the thermocline, provoking a decrease of the exergy of the system. The chosen solid media is fundamental to the formation and the stability of the thermocline [17].

An analytic approach proposed by Prof. Chiavazzo (Politecnico di Torino, Energy storage class) to calculate the stratification is the exergetic ratio (1):

$$\frac{\boldsymbol{\theta}}{\boldsymbol{\theta_m}} = \frac{\boldsymbol{T_m - T_0 - T_0 \ln\left(\frac{T_e}{T_m}\right)}}{\boldsymbol{T_m - T_0 - T_0 \ln\left(\frac{T_m}{T_0}\right)}} \qquad (1)$$

where:

$$T_m = \frac{1}{H}\int_0^H T(h)dh \tag{2}$$

and

$$\ln(T_e) = \frac{1}{H}\int_0^H \ln(T(h))dh \tag{3}$$

The higher is the exergetic ratio, the better is defined the thermocline, the higher is the exergy of the system. If $\frac{\theta}{\theta_m} = 1$ means that the TES is at a homogeneous temperature, the worst scenario we can achieve.

An interesting simulation on how standby the operation affects the thermocline stability of the PBTES is given by [4]: in figure 4 we can see how in an air-magnetite rocks PBTES the thermocline in the graph at left is about 40% of the height (biggest exergetic ratio), the time makes the temperatures become less stratified lowering the available energy of the system (lower exergetic ratio). A lower thermal conductivity slows the thermocline degradation.

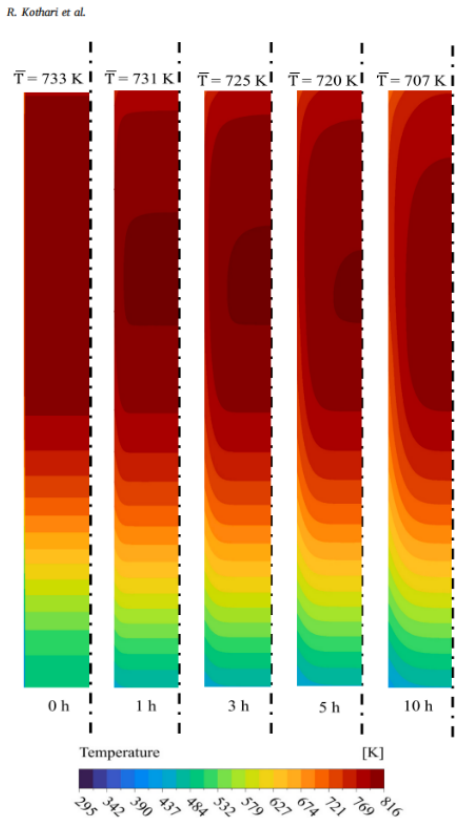

Figure 4 thermocline degradation

1.1.3. The computational models used

Esence et al. [21] conducted one of the most comprehensive reviews of numerical modeling approaches for PBTES. The authors classify models according to the degree of simplification: from the classical Schumann model (1D, two-phase) to advanced two-dimensional and intraparticle conduction models. Simplified 1D single-phase models are computationally fast and suitable for large-scale simulations, but they neglect temperature gradients inside solids and detailed wall effects. Two-phase Schumann-type models capture fluid–solid heat exchange realistically and are widely used in system-level studies, while three-phase or 2D models include wall conduction and radial gradients, improving accuracy at the cost of much higher computation time. Intraparticle conduction models become necessary when the Biot number exceeds 0.1, accounting for solid temperature gradients, though they increase CPU time by about an order of magnitude (figure 5).

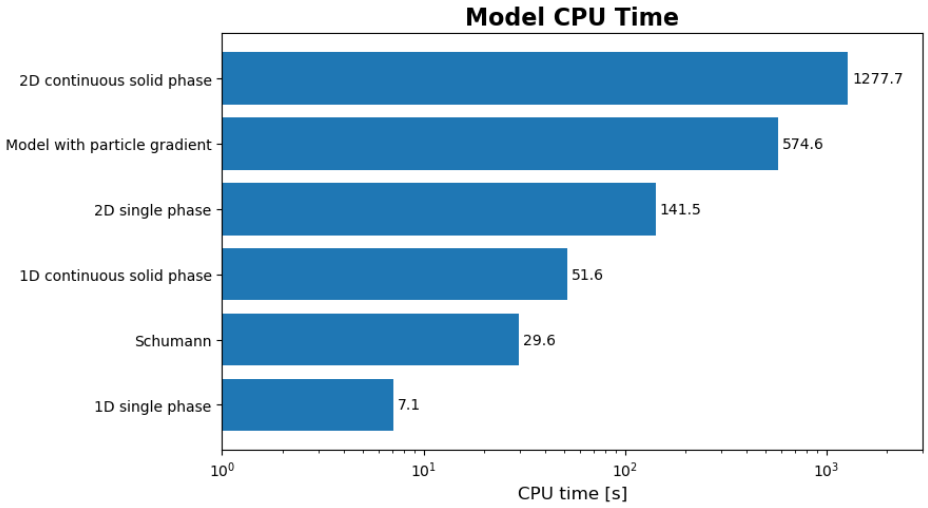

Figure 5 run time of different PBTES models

The review highlights that choosing the model involves a trade-off between fidelity and computational cost: simpler models suffice for system design and parametric studies, whereas detailed ones are required for transient, stratification, or high-temperature analyses. However, no existing model fully captures the behaviour of beds with mixed particle sizes or long-term mechanical effects, leaving scope for further development.

1.1.4. The history

The interest in PBTES has grown considerably with the expansion of mid- and high-temperature solar thermal power plants. Since the 1970s, several experimental campaigns and pilot projects have been carried out to evaluate its feasibility and scalability in CSP environments. The earliest pilot tests, such as the one by Hallet and Gervais [22], were followed by the first large-scale industrial installation at Solar One in 1982. Although that project was eventually decommissioned due to operational

challenges, it provided key reference data for the design of industrial-scale thermal storage tanks and system integration. These pioneering efforts laid the foundation for subsequent research on materials, cycling performance, and scale-up strategies, which continue to evolve today. Although the project was prematurely shut down due to operational issues, it provided a key reference for industrial-scale tank dimensions. A more robust experimental foundation was later provided by the work of Pacheco et al. (2002)[23], whose results are still widely used today. From around 2010 onward, research increasingly focused on operational cycling behaviour, thermo-mechanical constraints, and scale-up issues. Notably, Zanganeh et al. [24] demonstrated the feasibility of high-temperature rock beds with air, leading to the first commercial PBTES used in CSP since Solar One. In parallel, alternative designs like structured brick beds were investigated by Kuravi et al.[25], while significant efforts by CEA produced stable and repeatable thermal performance across different flow and temperature conditions. Moreover, Cascetta et al. [20] contributed to the understanding of geometric, flow, and wall thermal inertia effects, using alumina PBs operated with air. Finally, numerous laboratory-scale setups have supported the study of specific physical phenomena, though their limited representativeness highlights important scaling effects when compared to industrial systems.

In recent years, several commercial solutions for electrified thermal energy storage (TES) have been developed to support the decarbonization of high-temperature industrial processes. 1414 Degrees has introduced the SiBox® system, which stores latent heat in molten silicon (melting point 1414 °C) and can supply hot air up to 900 °C, with potential cogeneration applications [26]. Antora Energy utilizes solid carbon blocks heated resistively to approximately 2400 °C, from which thermal energy can be converted into electricity using thermophotovoltaic (TPV) cells [27]. Brenmiller Energy developed the bGen™ system, based on crushed rocks for sensible heat storage, charged by electricity or waste heat and discharged as steam or hot air up to 650 °C [28]. Electrified Thermal Solutions designed the Joule Hive™ Battery, consisting of electrically conductive refractory bricks heated by Joule effect up to 1800 °C [29]. Kraftblock employs a granular recycled material capable of operating between 350 °C and 1300 °C with round-trip efficiencies above 95%. Kyoto Group commercializes the Heatcube, a molten-salt-based storage unit that delivers saturated or superheated steam at 150–300 °C with a round-trip efficiency exceeding 93% [30].Finally, Rondo Energy developed the Rondo Heat Battery, composed of electrically heated refractory bricks reaching 1500 °C and capable of releasing hot air or steam with daily heat losses below 1% [11].

1.2. Danish Electricity market

1.2.1. The liberalization of Danish energy market

Denmark's electricity market liberalization constitutes a benchmark case in Europe's transition from a state-controlled monopoly to a competitive and renewable-oriented energy system. Prior to 1996, the Danish power sector was organized as a set of local, vertically integrated monopolies operating on a non-profit basis, with the primary objectives of ensuring national supply security and providing electricity at cost. Under increasing pressure from European Union directives promoting an internal energy market and from regional developments in the liberalized Nordic markets, Denmark initiated a comprehensive restructuring process based on unbundling—the legal and institutional separation of generation, transmission, distribution, and retail activities. This reform aimed to foster market competition and guarantee non-discriminatory access to the electricity grid.

A central element of this transformation was the establishment of a neutral Transmission System Operator (TSO) to manage the high-voltage network. Following the 2004 reform, the two regional TSOs were merged into Energinet, a fully state-owned entity ensuring grid neutrality and transparent market operation. To facilitate the transition and mitigate financial risks for incumbent generators, the government implemented a compensation scheme of approximately €1.2 billion for stranded costs.

The liberalized framework introduced a day-ahead market in which electricity prices are determined hourly based on supply and demand bids, integrating Denmark into the broader Nordic and European electricity markets. This structure significantly enhanced efficiency, competition, and the integration of variable renewable energy sources. As a result, wind and solar power currently supply more than half of the national electricity demand. However, retail market liberalization has progressed more slowly due to limited consumer incentives and the predominance of fixed charges in household electricity bills. Overall, Denmark's experience demonstrates that effective unbundling, the creation of an independent TSO, and regional market coupling are key enablers for a competitive and decarbonized electricity system [6].

1.2.2. Energy mix and wind power development

Danish total energy supply is characterized by a significant majority of petroleum-based products, which account for about 36% of the total, followed by natural gas (9.2%), coal and coal byproducts (3.2%) (IEA). Renewables (wind, solar and others) are about 14.9% of the total energy mix. The country has set ambitious climate goals: carbon neutrality in 2045 and a 110% emission reduction within 2050 (IEA). Denmark is betting on technologies as offshore wind, biomethane, hydrogen and carbon capture and storage to achieve the transition. Even if petrol-based products are still the biggest share, the role of renewables

is increasing constantly, highlighting a clear commitment to low emissions systems and advanced renewable infrastructures [31], [32].

The most renewable dependent system in Denmark is the electricity sector, with an outstanding 54% of electricity produced by wind power, 23% by bioenergy, and less than 1% produced by coal and oil (IEA). With over 80% of electricity produced by renewable resources, Denmark is one of the world leaders of the electricity transition. the national goal is to achieve the 100% of renewable electricity within 2030; however, this target is unattainable without adequate energy storage infrastructure, capable to stabilize and ensure a reliable the use of renewables in the grid. From this perspective the wind power combined together with an energy storage infrastructure which provide proper immediate power to the grid and a big capacity of storage can lead to the goal proposed in a reasonable timeframe [31], [32].

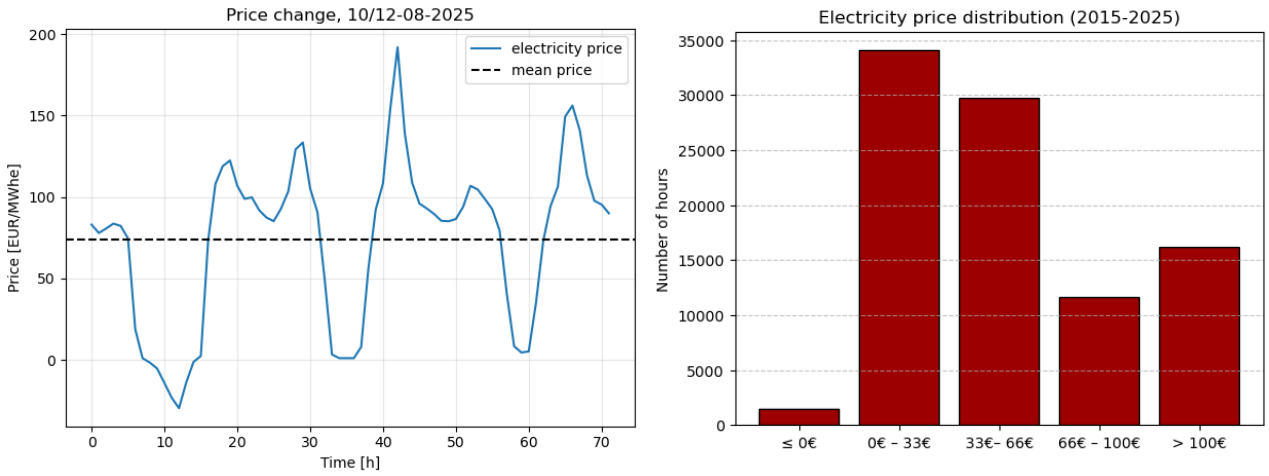

Figure 6 A-B, price per MWh in Denmark

Wind power, being intermittent and essentially cost-free to generate once turbines are built, has a profound influence on Denmark's electricity price formation. In general, high wind generation drives prices down, while low wind leads to higher prices. This is evident in the hourly Nord Pool market: when storm fronts or windy conditions boost output, Denmark often exports excess power and the local price falls relative to neighbouring areas. In extreme cases, the price can go negative, meaning producers pay to dispose of surplus energy. According to the Danish Utility Regulator, 2024 saw an unprecedented number of negative-price hours – 375 hours in West Denmark (DK1) and 275 hours in East Denmark (DK2) (27% increase compared with 2023) – due to the continued expansion of renewables (especially a jump in solar capacity) (figure 6 A, B). Such negative prices typically occur overnight or on weekends when winds are strong, but demand is low. They signal generators (particularly flexible ones) to reduce output and encourage consumption (or storage) to soak up the excess power. Conversely, during low-wind

conditions, Denmark's reliance on wind can contribute to price spikes if demand must be met by more expensive sources or imports. Denmark has relatively limited dispatchable capacity now (excluding wind/solar, available domestic generation is less than peak load), so during lulls in wind the country depends on importing electricity from neighbours or ramping up thermal units [6].

1.2.3. Electricity grid and infrastructures

Denmark's electricity infrastructure is marked by a strong transmission grid managed by the TSO Energinet and a decentralized network of distribution grids operated by regional DSOs. The transmission network consists of high-voltage lines at 400 kV (forming the backbone or "motorways" of power flow) and sub-transmission at 132–150 kV, interconnecting power plants, major load centers, and cross-border links. Notably, Western and Eastern Denmark are linked by the Great Belt HVDC cable (600 MW), opened in 2010 to connect the previously separate grids. Denmark is highly interconnected internationally: West Denmark has AC lines to Germany and multiple HVDC interconnectors (to Norway, Sweden, the Netherlands, etc.), while East Denmark connects via AC to Sweden and HVDC to Germany. These interconnections are crucial for integrating wind power and maintaining supply security. The distribution system in Denmark delivers power from the transmission grid to end consumers at medium and low voltages. There are dozens of local DSOs (reduced from over 200 before liberalization to 43 by 2019 through consolidation). DSOs are responsible for 0.4 kV to ~50 kV networks that supply households, businesses, and industries in their areas. While transmission is fully state-owned (Energinet), distribution companies are typically cooperatively or municipally owned, operating as regulated monopolies. Denmark has been modernizing its grid infrastructure – for example, moving much of the 150 kV/132 kV network underground for reliability and aesthetic reasons, and installing smart meters nationwide to enable advanced grid management. Overall, the country's grid infrastructure is robust and advanced, facilitating Denmark's high renewable penetration and cross-border electricity trade [6].

Chapter 1: RQ1

1.1. Problem definition

The formulation of the research question allows us to clearly outline the scope of the problem addressed and to specify the assumptions necessary to make a fixed-bed thermal storage system modellable under different operating conditions. The main objective is to assess whether a PBTES system is more suitable for dynamic operation, or whether its optimal performance is achieved in short-term or long-term seasonal operation. This temporal division is not simply an operational aspect, but directly determines the dominant thermo-fluid dynamic phenomena, the evolution of internal thermal stratification, and the overall sizing of the tank.

In the general picture, long-term seasonal operation has only been the subject of a preliminary assessment, as it is well documented in the scientific literature and already characterized by established models. Long-term systems have slow dynamics, deep cycles, and the need to minimize dispersion over time scales of weeks or months, conditions that are already well defined in the main reference studies.

Instead, RQ1 focuses in depth on two operating scenarios that are particularly relevant in the contemporary industrial context: short-term operation and dynamic operation. In the short-term case, the system is subjected to complete charge and discharge cycles, lasting several hours and with a regular pattern, such as to generate a repeatable and relatively stable thermal stratification (figure 7-A). In this regime, charging is carried out using hot air, a condition that allows the role of the thermophysical properties of the solid

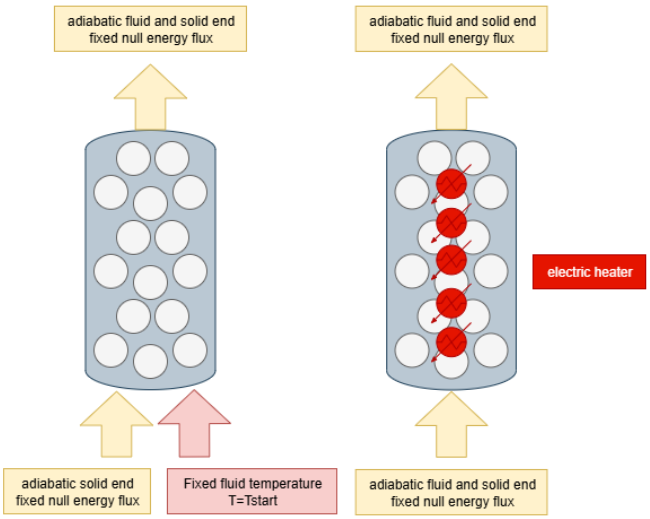

Figure 7 A (left) Sensible PBTES charged through mass flow rate - 7 B (right) Sensible PBTES charged through an electric heater

material, the efficiency of heat exchange, and the speed of propagation of the thermal front to be investigated.

The second axis of RQ1 concerns dynamic operation, which is much more complex from an operational point of view. In this case, the cycles are incomplete, activated or interrupted in response to external signals such as intermittent availability of renewable electricity, changes in energy prices, or the discontinuous presence of recoverable hot fumes. Charging is primarily carried out by means of an electric heater (figure 7-B), generating a modulable thermal pulse capable of following power profiles that vary over time. This mode is closely inspired by the actual operation of Rondo [11] systems, which use direct conversion of electrical energy into heat to maximize the operational flexibility of TES in industrial applications and in integration with high-penetration electrical grids.

The thesis draws inspiration from the Rondo system to analyse this system, highlighting three fundamental elements:

1. the dual-media technological configuration, with air as the carrier fluid and spherical solid material for storage.
2. the hybrid charging mode, thermal and electrical.
3. the declared characteristic powers, approximately 20 MW electrical input and 7 MW thermal output, which represent a realistic order of magnitude.

Since much of the detailed information is not public, the model developed integrates this data with assumptions derived from the literature—such as porosity, temperature range, environmental conditions, material properties, and insulation thickness—together with values optimized during numerical simulations.

The combined definition of these assumptions allows for a quantitative study of the effects of sphere diameter, solid material properties, tank geometry (height, diameter, and aspect ratio), and system capacity. By comparing short-term and dynamic data, and keeping long-term data as a theoretical reference, it is possible to rigorously answer the initial question, identifying which PBTES configuration is most suitable for each operating regime, and which design compromises emerge from the thermal and fluid dynamics analysis.

1.2. Methodology

1.2.1. Model description and explaining of the terms:

The thermal behaviour of the PBTES system is described through a one-dimensional, two-equation model accounting separately for the fluid and solid phases along the axial direction of the bed. The formulation captures the dominant heat transfer mechanisms occurring during both charging and discharging operations, namely transient energy storage, axial transport, interphase heat exchange, and thermal losses to the environment.

Fluid phase energy balance

The energy balance for the fluid phase is expressed as:

$$\boldsymbol{\varepsilon \rho_f c_{p,f}\left(\frac{\partial T_f}{\partial t}+u\frac{\partial T_f}{\partial z}\right)=\frac{\partial}{\partial z}\left(k_{f,\mathrm{eff},z}\frac{\partial T_f}{\partial z}\right)+ha_s(T_s-T_f)+Ua_b(T_\infty-T_f)} \quad (4)$$

The transient term $\varepsilon\rho_f c_{p,f}\frac{\partial T_f}{\partial t}$ represents the temporal variation of the internal energy of the fluid occupying the bed porosity, weighted by the void fraction ε. The convective term $\varepsilon\rho_f c_{p,f}u\frac{\partial T_f}{\partial z}$ accounts for axial energy transport induced by the fluid velocity and governs the propagation of the thermal front, especially under dynamic or fast charging conditions. Axial conductive transport $\frac{\partial}{\partial z}\left(k_{f,\mathrm{eff},z}\frac{\partial T_f}{\partial z}\right)$ is modelled through an effective thermal conductivity, which incorporates the effects of tortuosity and geometric constraints imposed by the packed structure and contributes to the attenuation of steep temperature gradients. The radial conductive contribution is neglected due to the monoaxiality of the model used, described in 1.2.2 and 1.2.3.

The interphase convective heat transfer term $ha_s(T_s-T_f)$ describes the energy exchange between the fluid (f) and the solid (s) particles and constitutes the core mechanism enabling sensible heat storage and retrieval. Finally, thermal losses to the surroundings $Ua_b(T_\infty-T_f)$ are modelled through a global heat transfer coefficient and an equivalent surface-to-volume ratio, accounting for conduction through the vessel wall and insulation as well as external convection and radiation. These losses become increasingly relevant at the high operating temperatures typical of air-based PBTES systems.

Temperature-dependent thermophysical properties, interphase heat transfer correlations, effective conductivities, and geometric parameters of the PBTES are implemented according to the constitutive formulations reported in the reference model

adopted. A comprehensive description of these correlations and their experimental and numerical validation for PBTES applications is provided in [12].

Solid phase energy balance

The solid phase is governed by the following energy balance:

$$(\mathbf{1}-\boldsymbol{\varepsilon})\boldsymbol{\rho_s c_{p,s}}\frac{\partial \boldsymbol{T_s}}{\partial \boldsymbol{t}} = \frac{\partial}{\partial \boldsymbol{z}}\left(\boldsymbol{k_{s,\mathrm{eff},z}}\frac{\partial \boldsymbol{T_s}}{\partial \boldsymbol{z}}\right) + \boldsymbol{h a_s}(\boldsymbol{T_f}-\boldsymbol{T_s}) + \ddot{\boldsymbol{\phi}} \qquad (5)$$

The accumulation term $(1-\varepsilon)\rho_s c_{p,s}\frac{\partial T_s}{\partial t}$ represents the temporal variation of the thermal energy stored in the solid matrix, which provides the dominant thermal inertia of the system. The volumetric heat capacity of the solid phase therefore strongly influences the stability and shape of the thermal front during cyclic operation. Axial conduction within the solid matrix $\frac{\partial}{\partial z}\left(k_{s,\mathrm{eff},z}\frac{\partial T_s}{\partial z}\right)$ is described through an effective thermal conductivity that accounts for particle-to-particle contacts and internal heat diffusion.

The interphase heat transfer term $h a_s(T_f - T_s)$ ensures energy conservation between the two phases and mirrors the corresponding contribution in the fluid equation with opposite sign. The volumetric heat source term $\ddot{\phi}$ allows the inclusion of internal heat generation within the solid phase, such as direct electrical heating. This modelling feature enables the representation of hybrid or electrically heated configurations, enhancing the capability of the system to respond rapidly to dynamic operating conditions.

1.2.2. Numerical assumptions

From a numerical standpoint, the model relies on a set of simplifying assumptions that reduce the complexity of the problem while maintaining a physically consistent description of the system. The thermophysical properties of the solid material are assumed to be independent of temperature and are fixed at average values representative of the operating range. This choice makes the model lighter from a computational perspective, whereas the temperature dependence of the properties is introduced only during the validation phase to more accurately compare the numerical results with reference data.

The spatial formulation is reduced to a one-dimensional system, solving the temperature field solely along the axial coordinate of the bed. Radial gradients are therefore assumed negligible, and both the fluid flow and the solid–fluid heat exchange are represented in a cross-sectionally averaged form, consistent with the elongated geometry of the reactor and with the objective of describing the overall behaviour of the storage system.

Finally, heat losses to the surroundings through the tank wall are modelled using an “electric-like” approach, based on the analogy between heat fluxes and electrical currents. In this representation, heat dissipation is treated as a flux proportional to the

temperature difference between the system and the environment, mediated by an equivalent thermal resistance. This formulation, referenced in the review of interest, allows the effects of losses to be included compactly while remaining consistent with the one-dimensional structure of the model.

1.2.3. Discretization, boundary conditions and validation

The numerical model is based on a finite-difference discretization in space combined with an implicit backward Euler scheme in time. The same numerical approach is adopted in [16], 4.1.2 and Appendix C, to which the reader is referred for a detailed derivation of the finite-difference operators and the treatment of the governing equations. In the present work, the discretized equations are assembled in a slightly different matrix form; however, the resulting algebraic system is numerically equivalent and leads to the same physical behaviour and accuracy.

Application of the method to the governing equations

The fluid- and solid-phase energy equations are discretized along the axial coordinate of the bed, yielding a coupled system of algebraic equations at each time step. The backward Euler method is used to advance the solution in time, ensuring unconditional stability.

The model is closed by appropriate boundary and initial conditions, which differ depending on whether the internal electric heater is switched off or on.

Case 1 – Electric heater off:

- Inlet boundary condition: A fixed mass flow rate is imposed at the inlet, together with a prescribed inlet temperature $T_{\text{in}}(t)$. For the validation case, $T_{\text{in}}(t)$ is directly taken from the reference dataset and is approximately constant at the maximum operating temperature, except for the initial transient. For the additional tests, $T_{\text{in}}$is set to a constant value equal to T_{max} (Dirichlet b.c.).
- Outlet boundary condition: The outlet node is assumed adiabatic, implying zero axial heat flux at the end of the bed (Neumann b.c.).
- Initial condition: The temperature field in both phases is initially uniform and equal to the base temperature of the system, representing a fully cooled state prior to charging.

Case 2 – Electric heater on

- Inlet boundary condition: The inlet node is treated as adiabatic with respect to axial conduction (zero axial heat flux), while the mass flow rate is kept fixed. (Neumann b.c.).
- Outlet boundary condition: The outlet node is assumed adiabatic (Neumann b.c.).

- Initial condition: The entire bed is initialized at the minimum temperature of the operating cycle, corresponding to the "cold" state before internal heating begins, in *Chapter RQ2* will be clear how this condition represents the condition of recycling of the waste heat from the system and external sources.
- Heater activation region: For validation against the reference configuration, the volumetric heat source associated with the electric heater is activated only in the first 20% of the axial nodes. For the Rondo-like configuration, the heater is instead extended to the entire bed length (100% of the nodes), representing a fully internally heated PB.

The validation of the numerical model is based on two complementary references that allow assessment of the storage behaviour both during charging with hot air and in the presence of internal heat generation.

Validation

The first validation uses the experimental data of Cascetta[33], employed both for the charging phase (figure 8) and for multi-cycle operation (figure 9). In the first case, the objective is to verify the correct propagation of the thermal front and the consistency of the temperature profiles along the bed; in the second, to assess the model's ability to reproduce realistic operating conditions in which the system does not fully regenerate between one cycle and the next, namely short-term operation. This confirms the adequacy of the heat-transfer correlations and of the one-dimensional formulation adopted. This validation is quantitative, and the input data are made as similar as possible to those of the experiment reported in the paper.

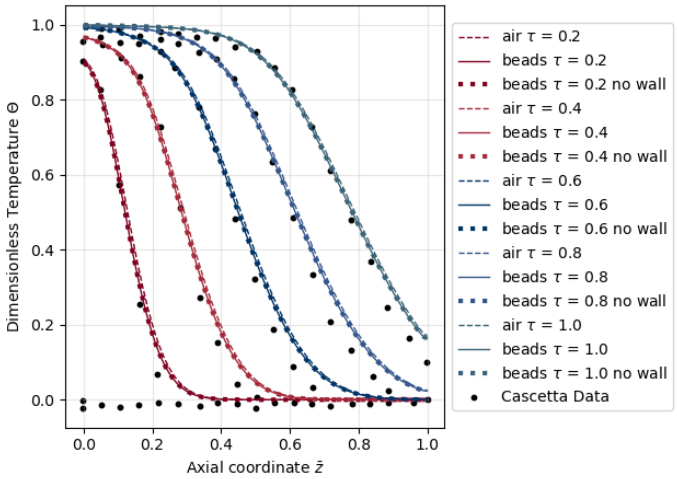

Figure 8 mono-cycle validation

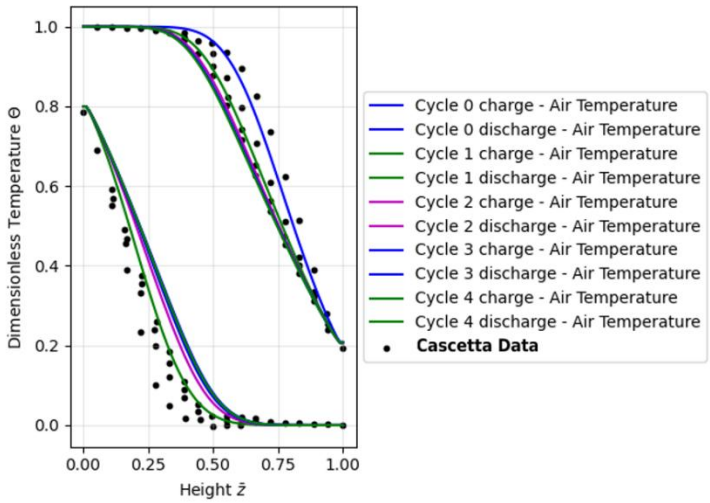

Figure 9 multi-cycle validation

The second validation refers to the electric-heating model developed by Silvia Trevisan [34](figure 10), which provides a consolidated description of internal heat generation via electrical heaters. Comparison with this model (figure 11) makes it possible to verify how accurately the simulation reproduces the interaction among the volumetric heat source, the solid's thermal dynamics, and the convective transport in the fluid—an essential condition for analysing fast, electrically driven charging scenarios. This validation is qualitative: the data from Trevisan's model were not reproduced to perform the comparison; instead, the correspondence of the characteristic regions in the temperature–height–time maps was examined. This approach validates not only the numerical model already benchmarked against Cascetta's experiment, but also the method used to implement the heat exchanger for next chapter (*RQ2*) PBTES full scale tests that form the core of the present research.

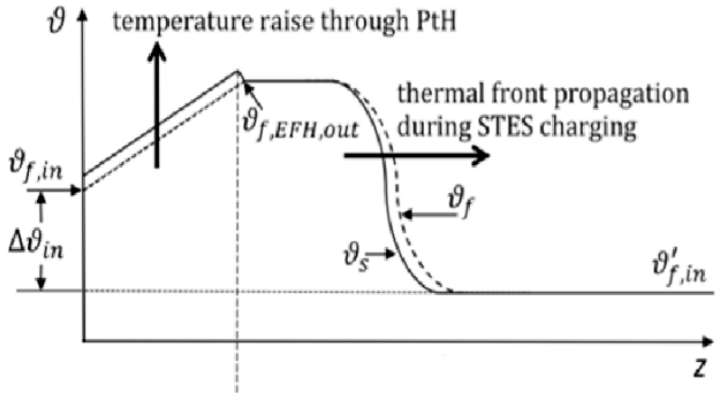

Figure 10 graph extracted from Trevisan's model

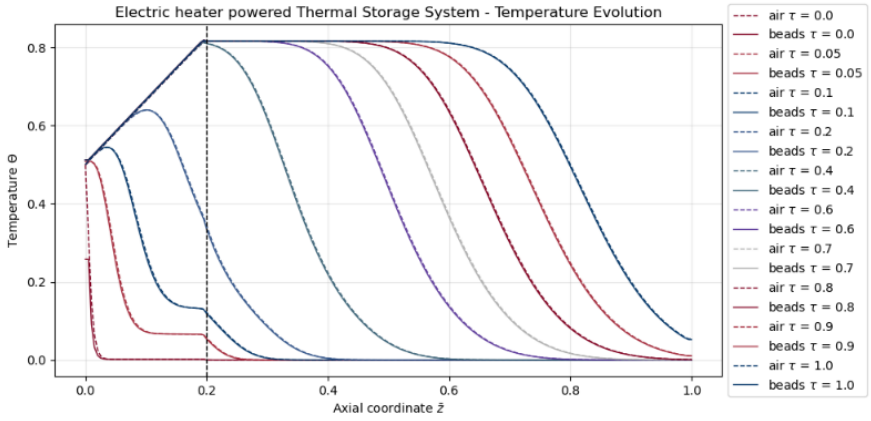

Figure 11 Model validation

1.2.4. Materials properties

In the preliminary comparison between different classes of materials, it emerged that each category has advantages and limitations directly attributable to its thermophysical properties and procurement costs. Ceramic materials generally offer excellent performance in terms of stability at high temperatures, mechanical strength and ability to maintain their morphology unchanged after repeated thermal cycles; however, the high cost of production and processing limits their large-scale use. At the opposite end of the spectrum are industrial waste materials, which are the most economically favourable option, but exhibit marked variability in thermal properties and poor predictability of cyclic operation, which reduces their reliability for medium- to long-term applications. Metals, although characterised by high thermal capacity and excellent mechanical properties, have excessively high thermal conductivity, which tends to generate overly steep temperature fronts and inadequate thermal stratification within the bed. Natural rocks are the most widely used solution due to their low cost and a set of thermal properties that are adequate on average, although not always optimised for dynamic conditions or high temperatures.

For the numerical analysis, six solid materials were considered in Table 2, for which density ρ, thermal capacity $\rho \cdot c_p$ and thermal conductivity $k(T)$ were defined consistently based on the relationships and datasets reported in the *rhocpmat* and *kappa* functions. The following table summarises the materials used in the model, specifying their thermophysical properties and the form in which they were represented (constant in the temperature range or function of temperature via polynomial or cubic spline interpolation).

Table 2 Analysed material properties

Materials	**Density ρ [kg/m³]**	$\rho \cdot c_p\,(T)$ **[J/m³K]**	**k(T) [W/mK]**	**Ref.**
Allumina	3550	$\rho \cdot c_p\,(T) = 0.0022T^2 + 3.0637T + 65.5464$	$k(T) = 0.0001T^2 - 0.1773T + 79.925$	[33]
cycled magnetite	2600	Experimental values in tables	Experimental values in tables	[35]
Quartzite	2500	$\rho \cdot c_p = 2.07 \cdot 10^6$	$k = 3{,}155$	[35]
Basalt glass	3000	$\rho \cdot c_p = 2.03 \cdot 10^6$	$k = 1{,}6$	[36]
Reinforced concrete	2200	$\rho \cdot c_p = 1{,}87 \cdot 10\text{^}6$	$k = 1{,}5$	[36]
Cofalit	3120	$\rho \cdot c_p = 3{,}0 \cdot 10\text{^}6$	$k = 2{,}2$	[36]

1.2.5. Methods to quantify the PBTES performance

To ease the comparison among long-term, short-term and dynamic mode, the analysis focuses on two fundamental parametra, which allow for rigorous quantification of both the fraction of energy that can be delivered and the thermal quality of the energy supplied during discharge.

The first parameter, the utilisation ratio, expresses the ratio between the thermal energy actually available during a short-term cycle and the maximum energy that can be stored in the system.

$$\boldsymbol{R_u = \frac{E_{available}}{E_{max}}} \tag{6}$$

It quantifies the level of exploitation of the material's thermal capacity. Therefore, a value close to unity indicates that the behaviour of the system is similar to the full charge and discharge and with low losses, while lower values show the increasing penalization associated with a partial utilization, leaving big quantity of material not used and its properties not exploited.

The second parameter concerns tolerance *T*, which is directly linked to the cut-off temperature
T_{cut} , defined as the minimum temperature below which the energy can no longer be considered usable in the application context, this parameter is linked to the user, which decides the best compromise between the quality of the output and the optimization of the PBTES operation.

$$T = \frac{T_{cut} - T_{min}}{T_{max} - T_{min}} \quad (7)$$

The tolerance T describes how strong is the constraint of the outlet temperature: low t values correspond to more tolerant requirements, allowing energy to be extracted even at relatively modest temperatures, while high values reflect applications in which energy is considered useful only if delivered at close to the maximum temperature. From an operational point of view, T_{cut} therefore represents the threshold above which the outgoing heat flow can be sent to the user, characterising the quality of the energy supplied.

During the charging the same tolerance can be used to loose the least amount of energy, at certain point the mass flow rate will start to exit the PBTES at a temperature above the minimun temperature, and this will be considered as a loss, because the temperature is not high enough to be useful at that point the charging should end. The usage of a tolerance will increase the utilization ratio during charging and still ensure a quality output at any moment during discharge.

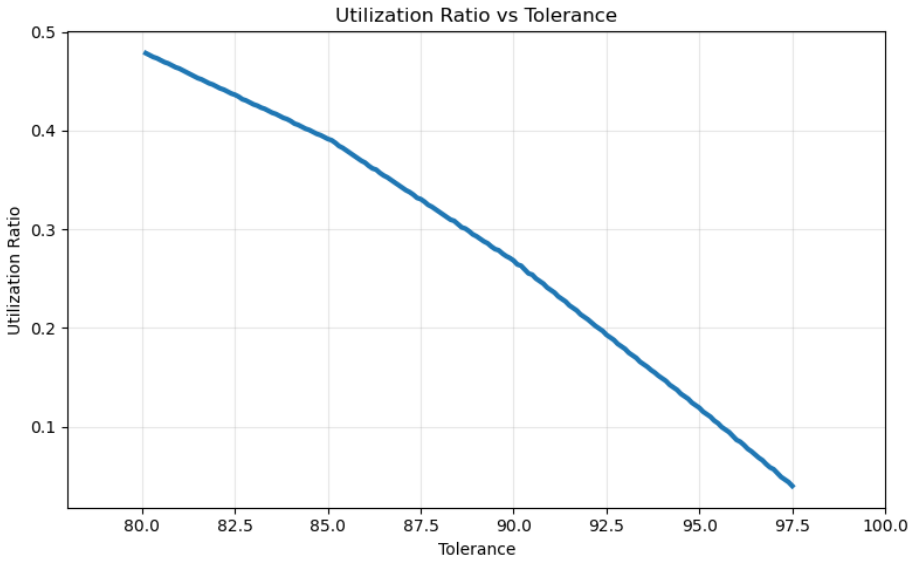

Figure 12 Utilization Ratio and Tolerance dependence

The combined analysis of tolerance and utilization ratio (figure 12) shows a clear linear trend: as the tolerance decreases, a larger fraction of the stored thermal capacity becomes exploitable, leading to a proportional increase in R_u. This relationship highlights how relaxing the minimum outlet temperature requirement directly enhances the effective usability of the storage during short-term operation.

1.3. Results

1.3.1. long term operation analysis

1.3.1.1. Charge and discharge, observation of the cut temperature.

In the following plots the results of the charging and discharging operation in long term operation are shown. For each, the temperature profiles are described both with graphs at constant time (figure 13.A - 13.B) and at given locations along the height of the tank (figure 13.C - 13.D).

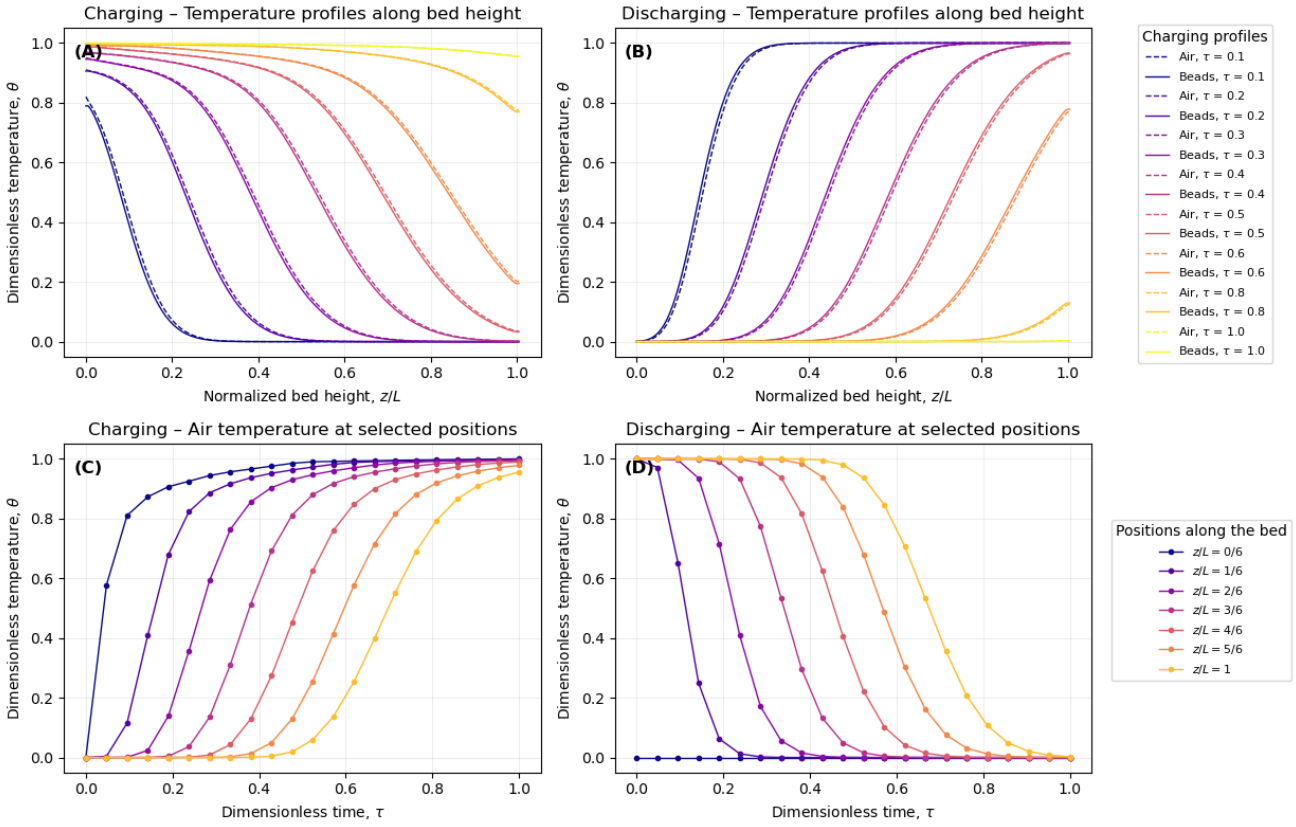

Figure 13 long term operation

The operation observed is a complete charge and a complete discharge, in figure 13.A - 13.B the thermocline formation and evolution is well highlighted, in figure 13.C - 13.D we can instead watch the cut off temperature in the z/L = 1 graph also the heterogeneity of the temperature is well visible, in fact the whole transient takes place in two line-graphs, resulting in about 1/3rd of the tank height.

1.3.1.2. Standby phase

Simulation and analysis of the insulation layer

The main research topic of this kind of operation is the standby operation, and the consequent loss of energy and so the standby efficiency due to the wall and ends losses. In our analysis the upper and lower ends are modelled as adiabatic, and the walls are modelled in accordance with figure 14, as an aluminium thin layer with a thicker insulation layer which is enough to give to the system a satisfying performance for our short-term operation analysis, whose results are shown in figure 15.

```
# data of wall losses
Rin=Din/2
spess1=13e-3
Rmid=Rin+spess1
kwall_1=45
spess2=100e-3
kwall_2=0.038
rhowall_2=32
cpwall_2=835
Rout=Rmid+spess2
```

Figure 14 Properties of walls

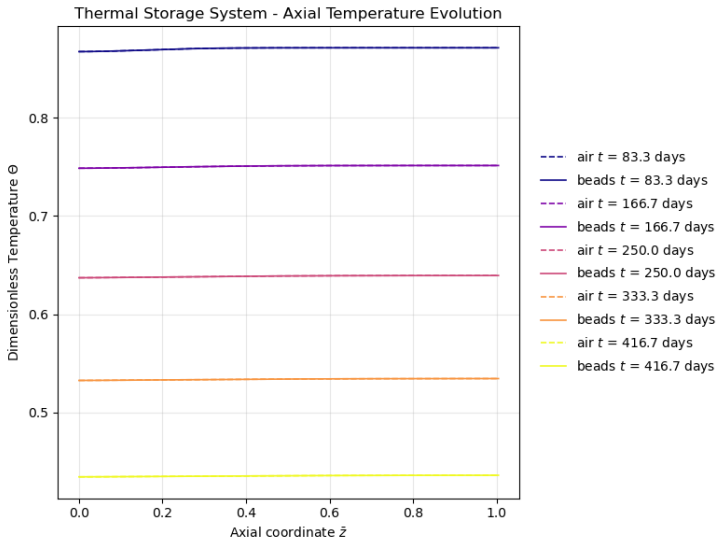

Figure 15 Stand-by operation simulation

1.3.2. Short term operation

1.3.2.1. Analysis of reference case

Next graphs (figure 16) are about the short-term operation, characterized by a behaviour that we will call thermal hysteresis similar to the hysteresis behaviour observed in ferromagnetic materials under variable magnetic field and also in non-perfectly elastic materials under variable force. The thermal hysteresis behaviour is

developed due to a temperature variation, in fact during the charge the inlet mass flow rate is at higher temperature than the discharge cycle, where the aim of the PBTES is to heat up the mass flow rate.

In figure 17.A the utilization ratio is shown which decreases with the cycles, figure 17.B shows the time needed for each charge and discharge, figure 17.C shows the state of charge of the system depending on the time. These charts are shown to clarify not only the heat transfer and so the temperature gradient changes in the tank, but also a point of view which is more practical on how much energy is stored and available in this kind of operation and how it changes with the time and the cyclic operations.

The efficiency of this operation will be observed in next paragraphs where it will be more contextualized, thanks to the comparison among the analysed parametra of geometry and operation.

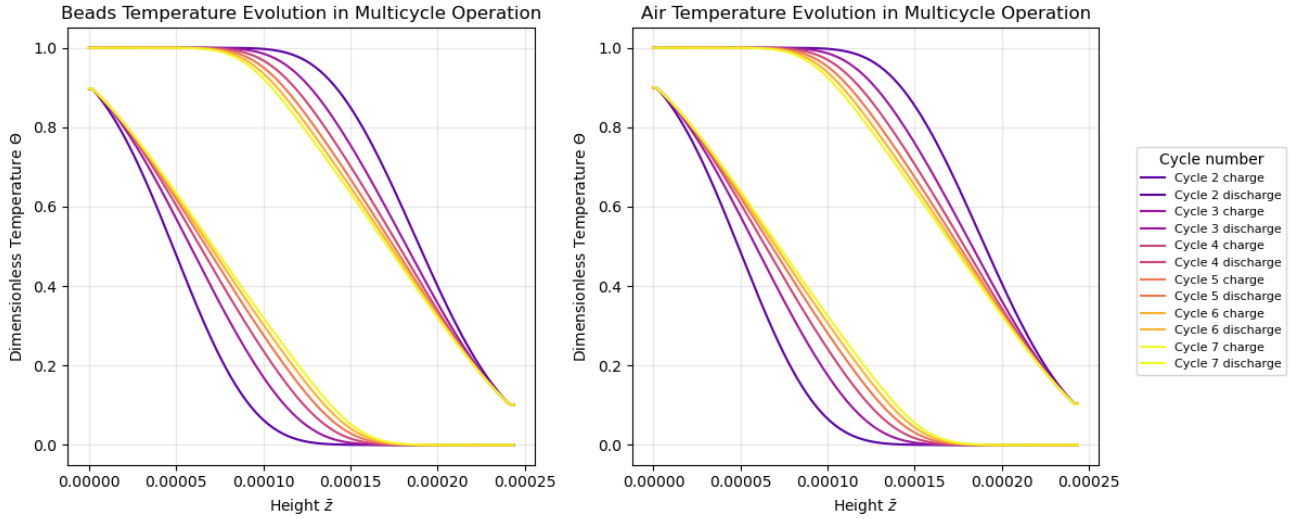

Figure 16 thermal hysteresis in short term operation

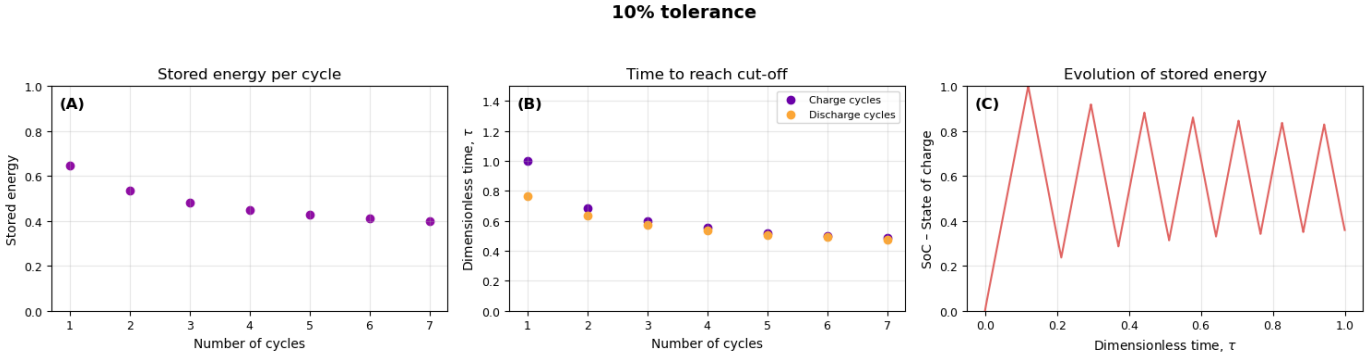

Figure 17 analysis on short term behaviour

The data shown to the end of the thesis are taken in pseudo steady operation, so after the end of the transitory part of the thermal hysteresis cycle, typically when the difference between the two consequent cycles energy stored is less than 1%. It is worth knowing that

in particular cases the pseudo steady state is not reachable, this behaviour is observed only in the 1% tolerance configuration: the materials in which this happens are not suitable for the usage in PBTES systems

1.3.2.2. Influence of the system geometry on its performance

- Aspect ratio change

The aspect ratio AR is the ratio between the height and the diameter of the tank. There are several studies which observe its influence on the operations [37] and all agree on the high importance of a proper dimensioning of the AR based on the operations of the system. From the following graphs (figures 18, 19, 20) the results are that the more the AR is high, so the higher and thinner is the storage, the more the thermal efficiency and the energy stored is. Thanks to this kind of choice the energy is distributed in a stratified way and the thermocline losses are lower.

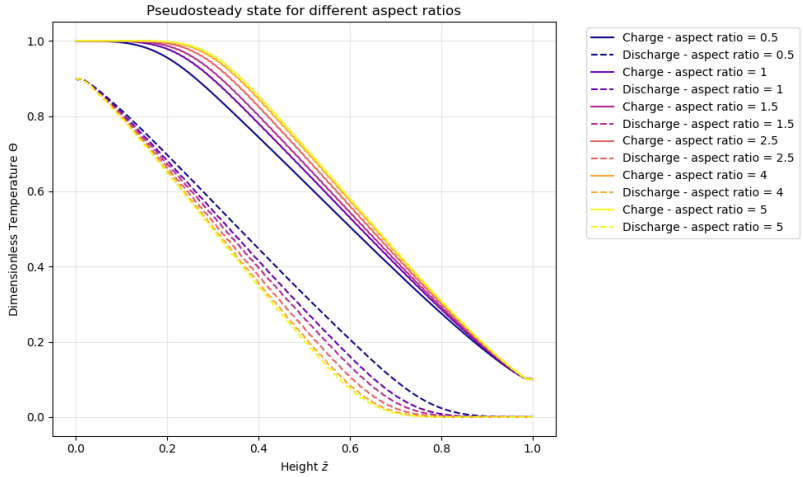

Figure 18 Temperature profile for different aspect ratio values

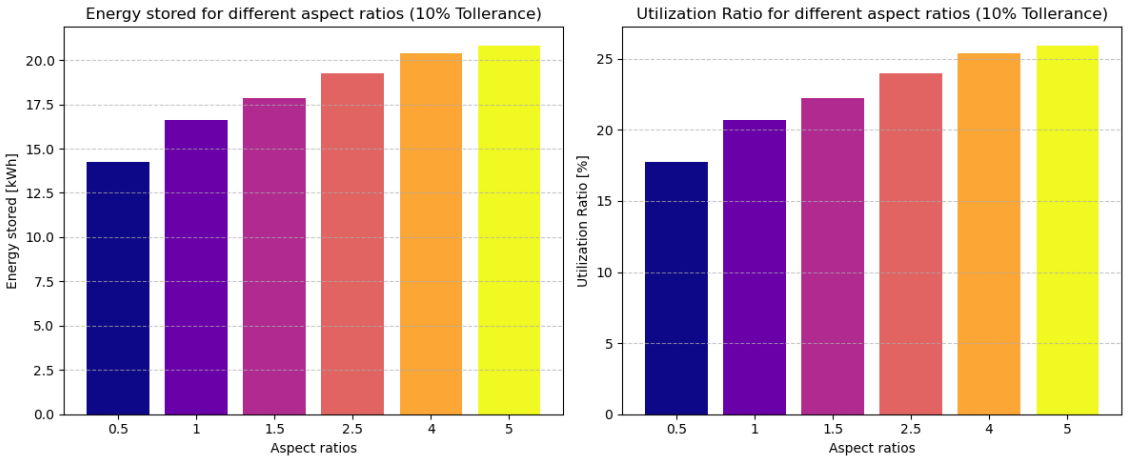

Figure 19 Energy Stored (left) and Utilization Ratio (right) for different aspect ratio values

The choice should consider also the structural side of the system, which is however part of this research and it will just be mentioned in chapter 2.2.1, during the economical evaluation of the tank's walls.

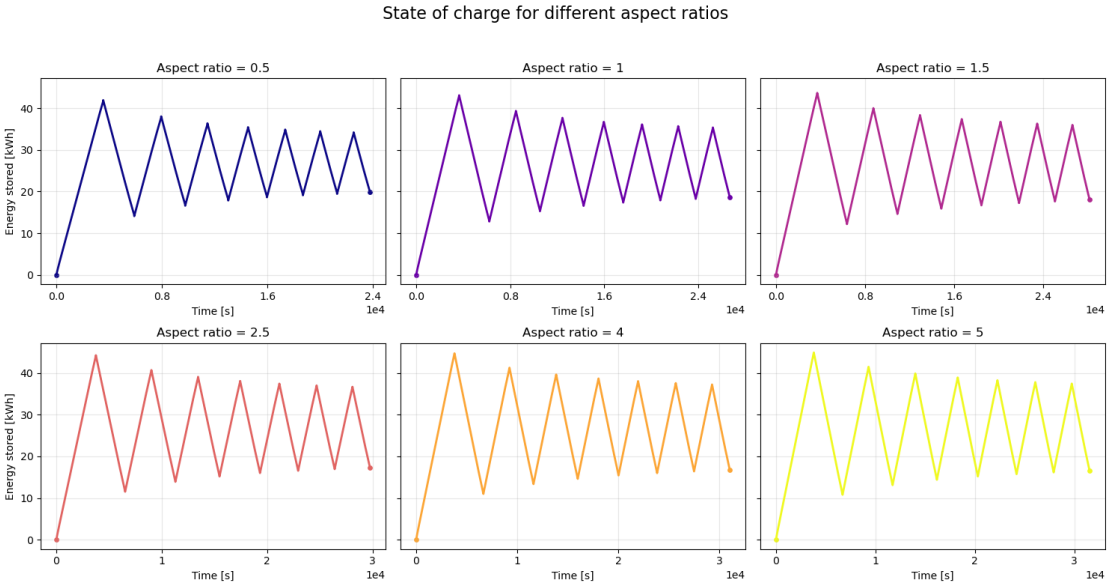

Figure 20 State of charge transient for different aspect ratio values

- Beads diameter change

The beads diameter is an important parameter, because the pressure drops depend on the bead's porosity and diameter. Since the porosity has been hypnotized fixed, the Ergun equation shows the relation between the pressure drop of the HTF and:

$$\frac{\Delta p}{L} = 150\frac{(1-\varepsilon)^2}{\varepsilon^3}\frac{\mu}{{d_p}^2}\,v_s + 1{,}75\frac{(1-\varepsilon)^2}{\varepsilon^3}\frac{\rho}{d_p}{v_s}^2 \;\propto\; \frac{1}{{d_p}^2} \tag{8}$$

The conclusion on this parameter has been made given the purpose of the research, which is not about the biggest thermal efficiency, but more about the return on the investment and the economic feasibility of the system, which in the RQ2 part is going to be modelled also in the auxiliaries. The results are shown in figure 21, 22, 23 and show an increase on the performance with the decrease of the diameter of the bead.

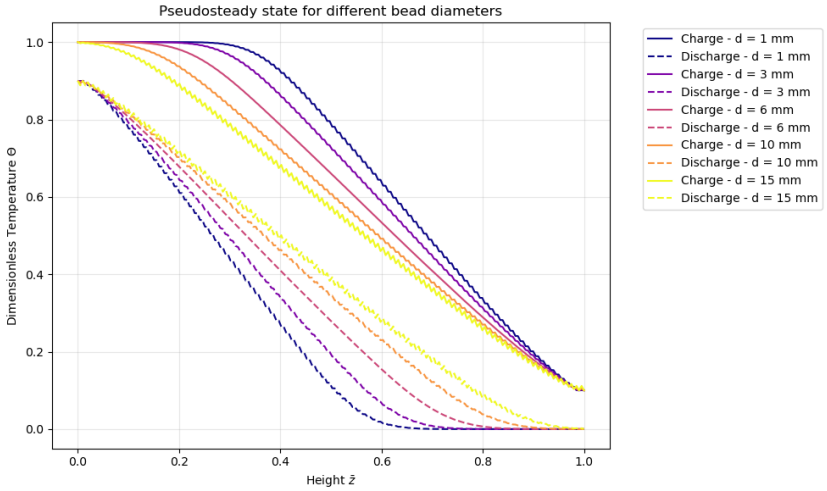

Figure 21 Temperature profiles for different beads diameter

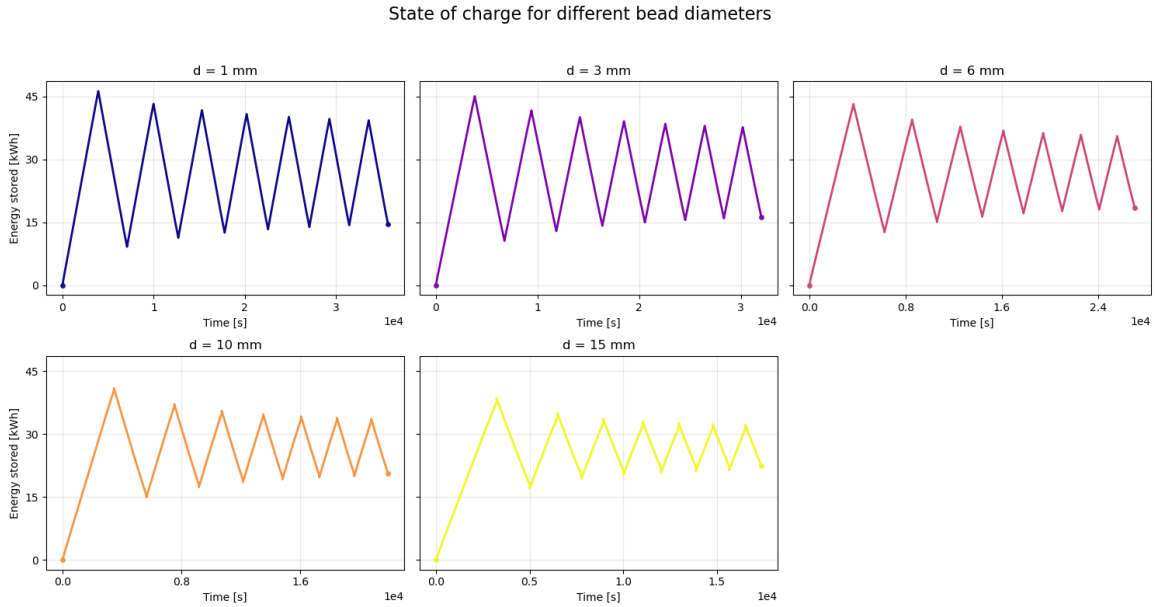

Figure 22 State of charge transient for different beads diameter

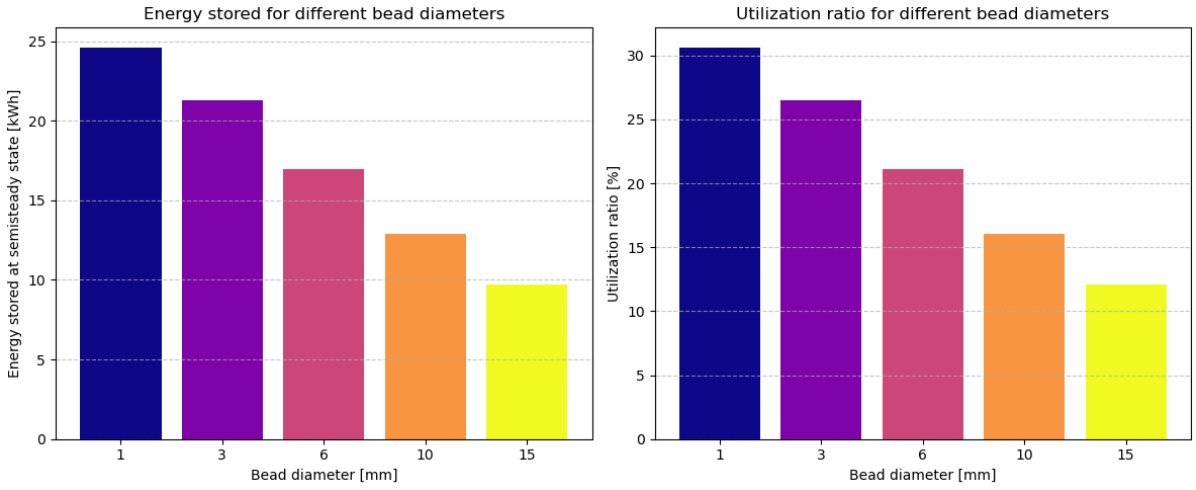

Figure 23 Energy Stored (left) and Utilization Ratio (right) for different beads diameter

- Volume change

The change in volume is another impactful parameter, figure 24, 25, 26 show a relevant increase in performance with the size of the tank. Keeping the other parametra constant, the energy available increases about 113% on a 100% increase on volume. In figure 21 there is also information about the increase in time happening by increasing the volume, and the fact that doubling the size from 4.8 to 9.6 m³ the charging time increases from 35000 s to about 37000 s means an increase of less than 6% in time.

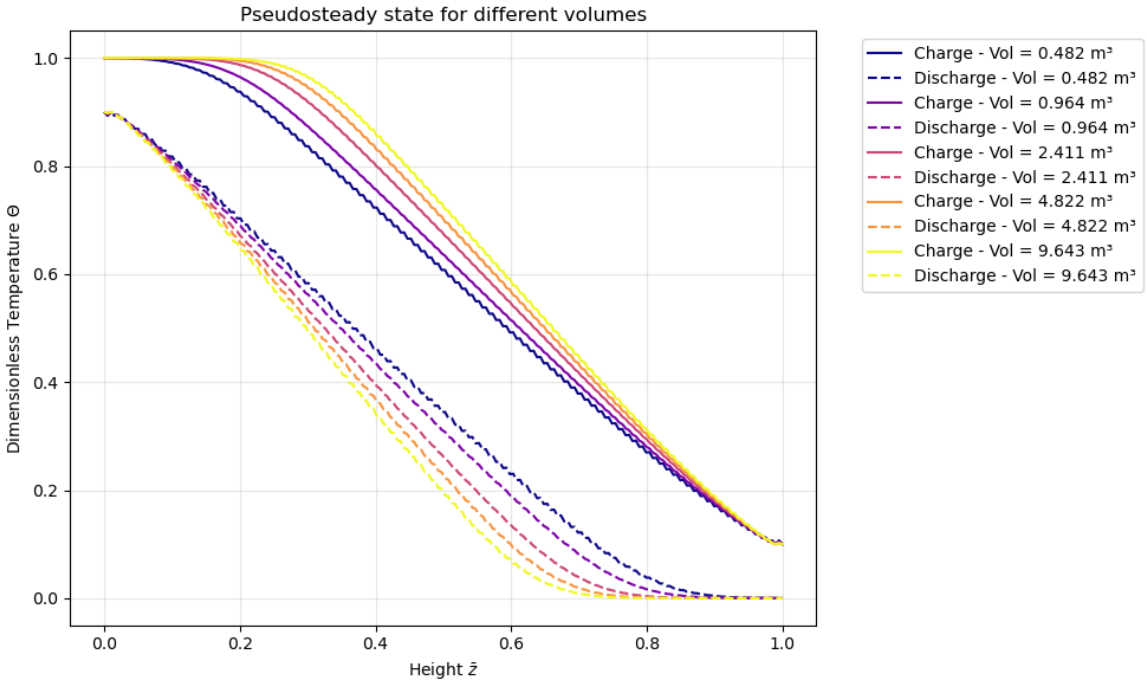

Figure 24 Temperature profiles for different volumes

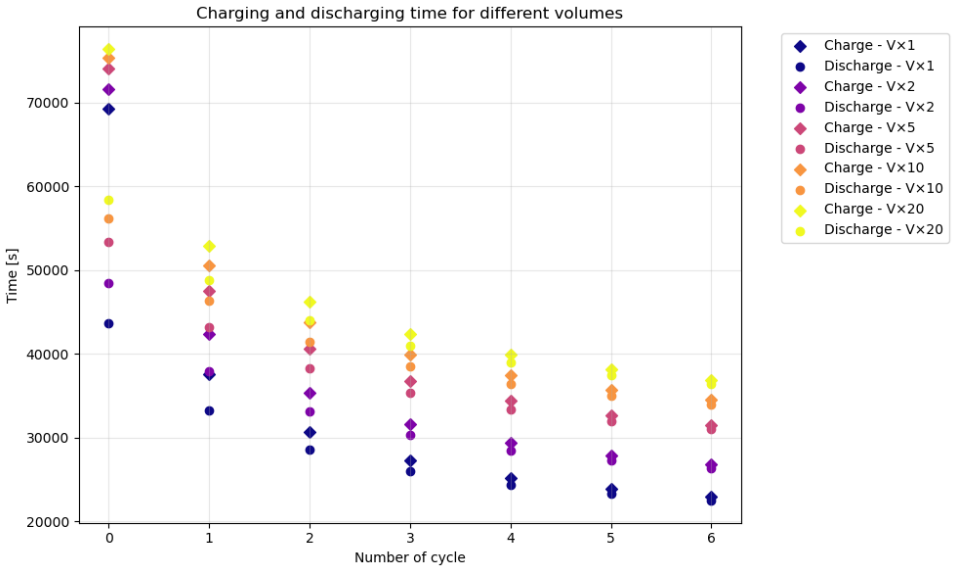

Figure 25 charging and discharging times for different volumes with validation simulation volume as reference

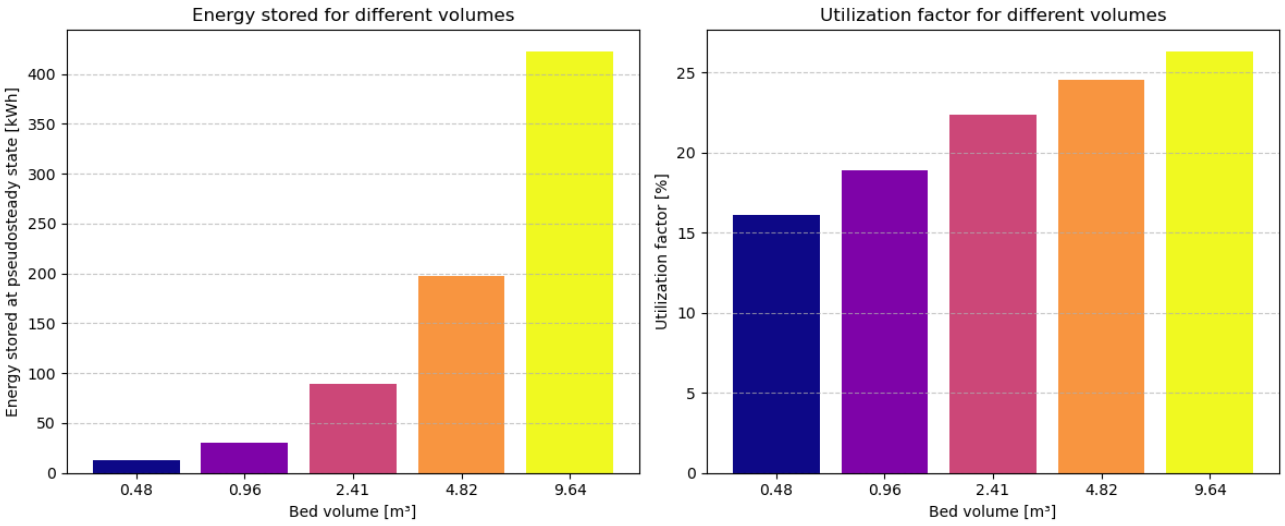

Figure 26 Energy Stored (left) and Utilization Ratio (right) for different volumes

1.3.2.3. Influencing of the material on the performance

Conductivity, capacity and convective heat transfer coefficient.

The materials used for the beads of the PBTES are crucial and may vary significantly their performance, as already stated in the methods section. From the following figure 27, 28 we can state that magnetite, according also with the latest studies (cited in the methodology) and applications is the most suitable for short-term, it is the most performative, this is because of its high thermal capacity and high operational temperature range. for the same occupied space there is more energy available to be used and a lower utilization ratio, thanks to its higher capacity: shown in figure 29 at mean temperature of conducted test. Its cost, comparable with the mineral materials is much lower than metallic and ceramic materials and it is a further confirm of the choice.

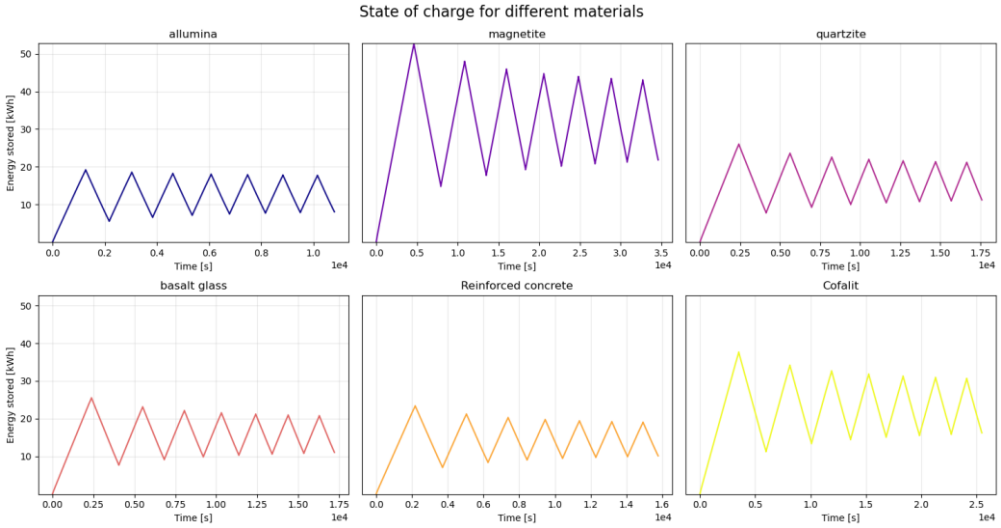

Figure 27 State of charge transient for different materials

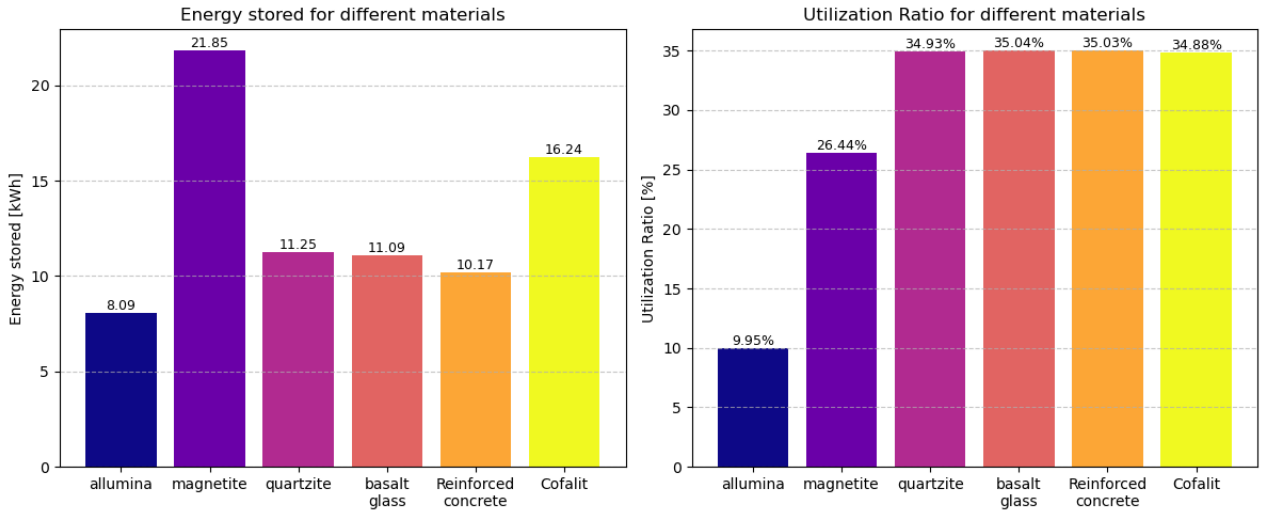

Figure 28 Energy Stored (left) and Utilization Ratio (right) for different materials

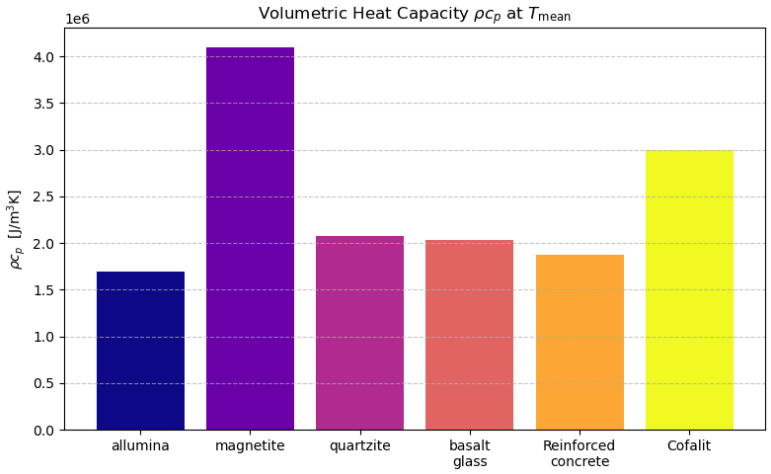

Figure 29 Volumetric heat capacity for different materials

1.3.2.4. Thermal hysteresis effect and tolerance

Tolerance has been kept fixed at 0.1 until now, next figure (figure 30) show how changing of a fraction of the temperature outlet and inlet in the system can enlarge of a relevant quantity the energy stored, in figure 31 is well shown how the tolerance is responsible for the stability of short-term operation, the graphs slope is bigger as low is the tolerance value: Reaching a pseudo steady state in a bigger number of cycles.

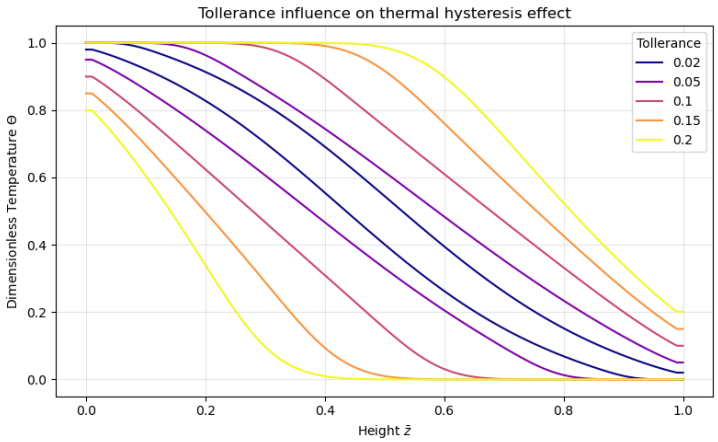

Figure 30 Temperature profiles for different tolerances

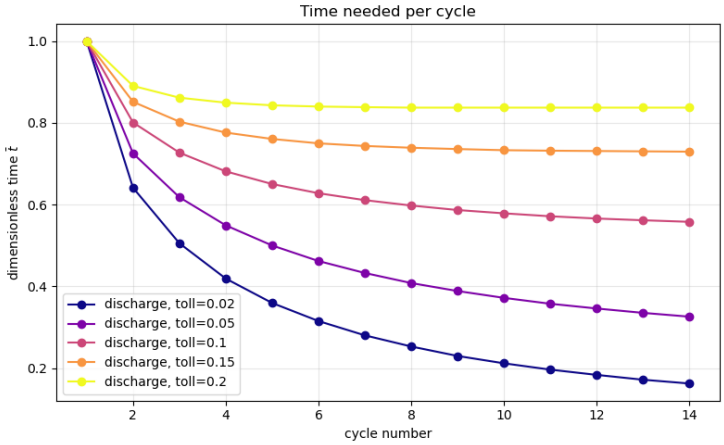

Figure 31 Time needed to complete initial cycles for different tollerances

1.3.3. Sizing, relation among volume, tolerance and energy stored.

This section presents the coupling between geometric, operational, and energetic aspects. Varying volume and tolerance, the energy stored in short-term operation changes widely. figure 32, 33 are fundamental for the choice of a proper geometry of the tank of the PBTES, when a given operation mode constrains the tolerance to a selected value.

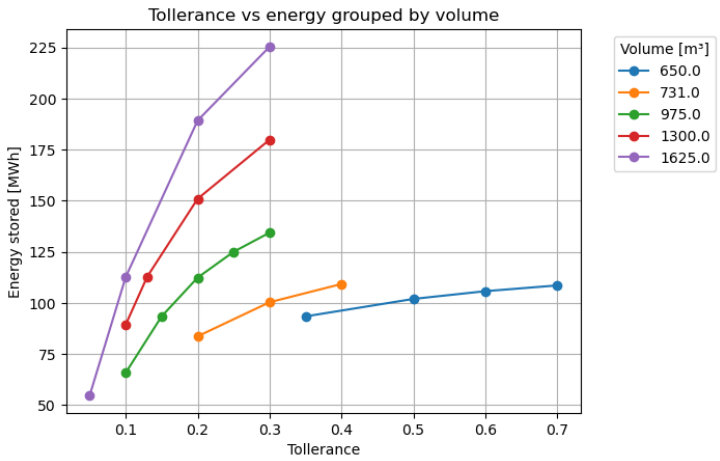

Figure 32 Relation between Tolerance and Energy Storage for different Volumes

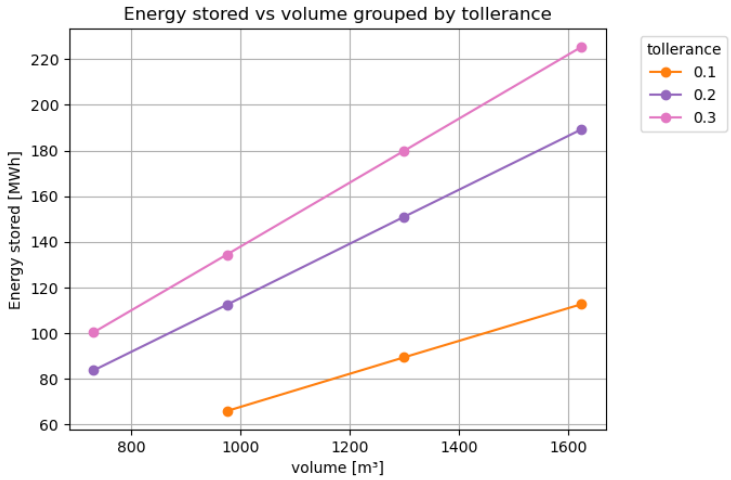

Figure 33 Relation between Volumes and Energy Stored for different Tolerance values

1.3.4. *Introduction of electric heater.*

The electric heater is simulated with different geometrical configurations and positions in order to identify the most effective solution. The version studied in this research is equipped with a safety system which turns it off when the temperature exceeds the maximum temperature of the system, this behaviour can be observed in figure 34 where the electric heater is located only on the first 20% of the PBTES height.

Also, a simulation with a distributed heat generation has been conducted, resulting in a homogeneous heating in the whole system, even with null air mass flow rate. The visual representation of this simulation is not included, as it does not provide additional insight, consisting of a simple monotonic trend reaching a steady-state plateau.

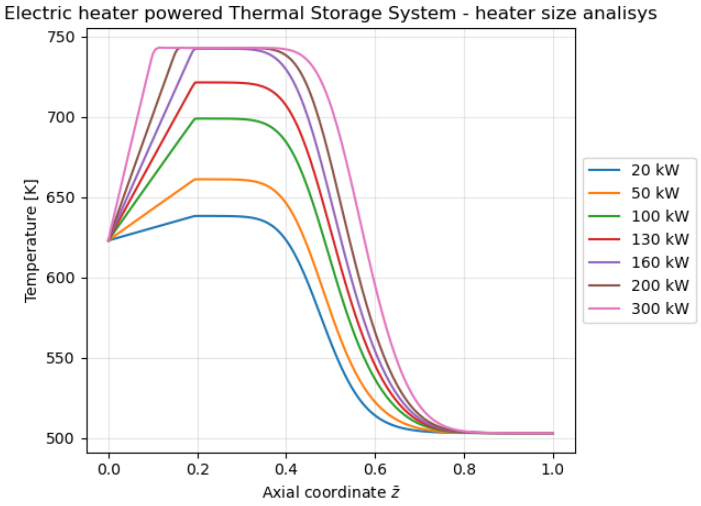

Figure 34 Temperature profiles at the same simulation time for different sizes of electric heater

1.4. Conclusions

1.4.1. Analysis of the different kinds of operations

In the 1.3.1 - 2 results section several graphs showing the simulation of typical PBTES operations are presented, from there we can analyse the main differences on performance:

- During seasonal operation, the storage is charged to its maximum level, retaining the heat stored for months, leading to thermal losses over time. The performance of the standby stage is therefore strongly dependent on the thickness and quality of the insulating layer. During the consequent discharge, a fraction of low temperature energy remains trapped in the storage, s the outlet temperature of the fluid falls below the minimum acceptable cut-off value.
  This type of operations results in an high utilization factor, thanks to the exploitation of most of the energy stored, and moderate thermal efficiency, because of the high wall and thermocline losses.
- During the cyclic operation the energy dissipated by the walls is reduced, due to the hours-to-days time of stand by operation. The energy trapped however increases, because now it is trapped both during charge and discharge. On the other hand the thermal efficiency is higher: the energy trapped during each cycle is lower and after some cycles it stabilizes achieving a near to 100% thermal efficiency. Despite this, there is often a utilization ratio which is near 30%.
- The dynamic behaviour is the one that exploits the PBTES properties the most. In the results section this operation mode has been not analysed numerically because of the high dependence on the volatility of the energy market in the input. As we will see in the second chapter, the thermal efficiency is high, close to the unity, thanks to the constant mass flow rate, which makes the energy stored in the system for low amount of time, the temperature level in the system is inhomogeneous, the lower part often discharges and recharges depending on the available energy supply, but the constant mass flow rate is able to supply high temperature air to the user with almost perfect quality of the output. This results in the best overall performance among the analysed regimes, showing the highest potential both the thermal efficiency and the utilization ratio.

1.4.2. The choice of geometry and material

The results in 1.3.2.2-3 give us valid parametra to size the system in an optimal way.

The volume analysis told that the bigger is the tank, the better performance it has, so the choice of using one single tank instead of more little ones has been taken.

The from the aspect ratio graphs I choose a AR=3 to size the shape of the cylindrical tank, this measure is valid because of the higher performance, without extremize the height of

the PBTES, that being a single tank has to remain in a reasonable shape to be supported by the foundation and be easily accessible during the manutentions.

The diameter of the beads has been chosen to be a compromise between energy stored and pressure drop, which affects the cost of the upstream compressor. Ergun Equation is plotted in figure 35 and the solution for the problem has been found with a compromise on performance and pressure drop, 8 mm diameter beads, a quantitative assessment of compressor power is performed in Chapter 2.

Lastly, the choice taken has been on the material: magnetite is the best compromise, ceramic materials are too expansive to be treated as a commercial industrial solution, the benefit on the performance does not justify the bigger price. Between the materials analysed in the results part magnetite has been selected as the more performative.

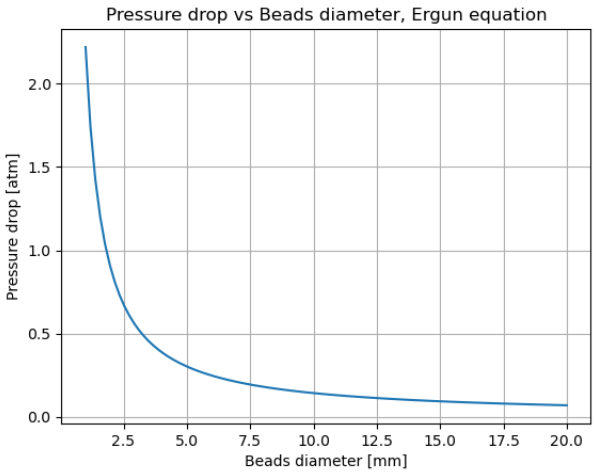

Figure 35 Ergun Equation, influence of beads diameter on pressure drop

1.4.3. Electric heater choice

The localization of an electric heater is crucial for the thermal efficiency of the storage. A localized heat source provides an inhomogeneous heating; this condition can be changed only by increasing the air mass flow rate. This behaviour, however, will generate a big loss of energy, because the air will flow out of the PBTES at a temperature between the minimum one and the cut off temperature for a relevant amount of time before becoming useful. The usage of a distributed electric heater, this phenomenon is the same seen in figure 12.C in the graph x/L = 1, in the case described in that paragraph this loss is due to the hot mass flow rate that enters the system at the opposite side of the PBTES. An electric heater installed all along the height of the system is a better choice, coupled with a null air mass flow rate. The thermal losses in this case are only due to the walls, negligible in short-term operation and with a proper insulating layer.

1.4.4. Final sizing

Coming to the final sizing, finalized for a PBTES to be used in dynamic behaviour, a constant air mass flow rate passes through the system dispatching energy at constant high temperature to the user, while the PBTES is being charged in different size time spans, (this will be deepened in the RQ2 chapter). The system volume should be determined based on the following considerations: a low tolerance parameter is acceptable, as dynamic operation allows for effective utilization of most of the storage capacity. The reference energy size is 100 MWh and following the figures 32, 33 this capacity is reached, with high tolerance at 700 m^3.

Chapter 2: RQ2

2.1. Problem definition

RQ2. What strategies can be applied to maximize the benefits of a PBTES system?

The second part of this thesis will face the problem to find the best strategies to maximize the benefits that a PBTES can have in an industrial context. The focus is now on the system that will embody the TES and how its operation can be valuable for the industry. The most suitable industrial frameworks for this kind of system have already been described in the State of Art [*State of Art, Chapter 1.1.1*] and the fundamental requirement which the dynamic behaviour can help handle is the supply of high temperature thermal energy, which must be stable, reliable and continuous. The thermal energy quality to be supplied to the used, is the main constraint, because the stability of the downstream operations depends on it.

In this context the PBTES is not a stand-alone system anymore, but it will be supported by a compressor, to contrast the pressure drops in the system, an heat exchanger for the supply of the output energy, and a heat exchanger to recover the energy from the same system and from external operations (figure 36).

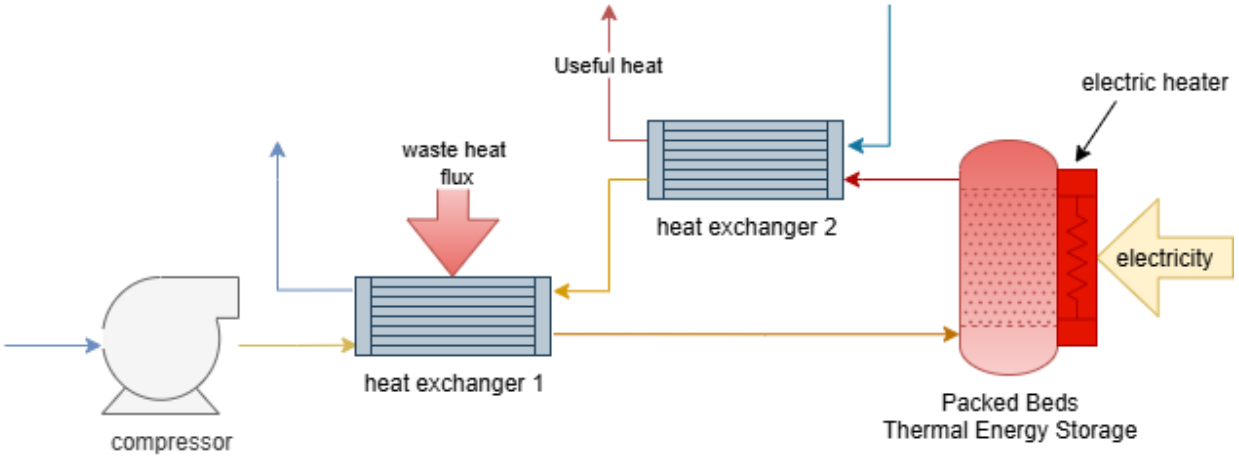

Figure 36 Complete Packed Beds Thermal Energy Storage system

The problem solved in RQ2 arises from the presence of strong fluctuations in the energy [*State of Art, chapter 1.2.2*] given by the unpredictable production of the renewable energy sources. The charging phase of the PBTES analysed is committed to an electric heater, so the economic value of this system highly depends on the electricity market conditions. The presence of low and negative prices lapses, together with the integration with local electricity production, maybe renewable gives the opportunity to charging strategies aimed to reduce the cost of the heat needed.

The strategy developed is based on the implementation of an algorithm based on the day-ahead electricity prices to buy electricity at the lower cost, and a photovoltaic farm to reduce the energy bought. The electricity will then charge the PBTES, and we expect that the air mass flow rate in output will have the same quality of a classical method for the heat production like a gas burner.

The last part of the analysis is going to evaluate the profitability of the system thanks to an economic analysis based on a data-based Net Present Value NPV and Levelized Cost Of Energy LCOE.

2.2. Methodology

2.2.1. Dimensioning of the PBTES system and gas-powered system comparison

Compressor

The dimensioning of the compressor has been made through the competences learnt in "thermal machines and structural mechanics" lectures by Professor Luciano Rolando, PoliTO

It is modeled as a multistage unit operating under steady-state conditions, with air treated as an ideal gas and thermodynamic properties evaluated at the environmental temperature. The inlet conditions are fixed at $p_{\text{in}} = 1 \times 10^5$ Pa and $T_{\text{in}} = T_{\text{env}}$. A constant isentropic efficiency $\eta_c = 0.8$is assumed for the compressor, and different configurations with a number of stages ranging from $n = 1$to $n = 4$are analyzed. The total pressure increase required by the system is uniformly distributed among the stages, leading to an equal pressure ratio for each compression stage.

Each stage is described by isentropic compression relations corrected for the compressor efficiency. The outlet temperature of a generic stage is calculated as

$$\boldsymbol{T}_{\text{out}} = \boldsymbol{T}_{\text{in}}\, \boldsymbol{\beta}_{\text{stage}}^{(\boldsymbol{\gamma}-\mathbf{1})/\boldsymbol{\gamma}} \tag{9}$$

while the corresponding specific compression work is given by:

$$\boldsymbol{w} = \frac{\boldsymbol{c_p}\, \boldsymbol{T}_{\text{in}} \left(\boldsymbol{\beta}_{\text{stage}}^{(\boldsymbol{\gamma}-\mathbf{1})/\boldsymbol{\gamma}} - \mathbf{1}\right)}{\boldsymbol{\eta_c}}, \tag{10}$$

where $\gamma = c_p/c_v$. The total specific work of the compressor is obtained by summing the contribution of all stages and is converted into shaft power by multiplying by the air mass flow rate. Finally, the investment cost of the compressor is estimated using a power-law scaling correlation [38]:

$$\text{Cost} = \mathbf{91562}\left(\frac{\dot{W}/\mathbf{10^3}}{\mathbf{445}}\right)^{\mathbf{0.67}}, \tag{11}$$

allowing the impact of the number of compression stages on both thermodynamic performance and economic cost to be consistently evaluated.

Heat exchangers

Both heat exchangers are modeled as shell-and-tube units using the same simplified thermal design framework. The heat duty is obtained from an energy balance with temperature-dependent properties,

$$\dot{\boldsymbol{Q}} = \dot{\boldsymbol{m}}\, \boldsymbol{c_p}(\boldsymbol{T}_{\text{mid}})\,(\boldsymbol{T}_{\text{out}} - \boldsymbol{T}_{\text{in}}) \tag{12}$$

The thermal driving force is evaluated through the logarithmic mean temperature difference,

$$\boldsymbol{\Delta T}_{\text{lm}} = \frac{(\boldsymbol{T_{h,\text{in}}} - \boldsymbol{T_{c,\text{out}}}) - (\boldsymbol{T_{h,\text{out}}} - \boldsymbol{T_{c,\text{in}}})}{\ln\left(\frac{\boldsymbol{T_{h,\text{in}}} - \boldsymbol{T_{c,\text{out}}}}{\boldsymbol{T_{h,\text{out}}} - \boldsymbol{T_{c,\text{in}}}}\right)}, \tag{13}$$

from which the required global conductance follows as

$$\boldsymbol{UA} = \frac{\dot{\boldsymbol{Q}}}{\boldsymbol{F}\,\boldsymbol{\Delta T}_{\text{lm}}}, \boldsymbol{F} = \mathbf{1} \tag{14}$$

The overall heat transfer coefficient is computed from the thermal resistance network, including internal and external convection, tube-wall conduction, and fouling,

$$\boldsymbol{U} = \left[\left(\frac{\mathbf{1}}{\boldsymbol{h_i}} + \boldsymbol{R_{f,i}}\right) + \frac{\boldsymbol{d_i}\ln(\boldsymbol{d_o}/\boldsymbol{d_i})}{\mathbf{2}\boldsymbol{k}_{\text{tube}}} + \frac{\boldsymbol{d_i}}{\boldsymbol{d_o}}\left(\frac{\mathbf{1}}{\boldsymbol{h_o}} + \boldsymbol{R_{f,o}}\right)\right]^{-\mathbf{1}}. \tag{15}$$

The convective heat transfer coefficients are evaluated using standard Nusselt correlations based on Reynolds and Prandtl numbers,

$$h = \frac{\mathrm{Nu}\, k}{d}, \quad \mathrm{Nu} = C\,\mathrm{Re}^{m}\mathrm{Pr}^{n}, \tag{16}$$

with coefficients selected according to the flow regime.

Finally, the required heat transfer area and the corresponding cost are obtained as

$$A = \frac{\dot{Q}}{U\,F\,\Delta T_{\mathrm{lm}}}, \qquad \mathrm{Cost} = 130\left(\frac{A}{0.093}\right)^{0.78}. \tag{17}$$

This formulation is applied identically to both heat exchangers, ensuring consistency in the thermal and economic assessment within the PBTES system

In the model, the pressure drops across the heat exchangers are deliberately overestimated to ensure smooth operation and a slightly pressurized outlet flow. A conservative value of 0.5 bar per pass is imposed, which is significantly higher than the values predicted by the sizing correlations. Using the same method, the calculated pressure drops are approximately 0.03 bar and 0.07 bar.

PBTES system

The cost estimation of the PBTES system [39] is performed using a simplified analytical approach, adopted due to the lack of consolidated economic scaling laws for this technology. The total TES cost is assumed to be dominated by two contributions: the pressure vessel and the solid storage material, consisting of alumina particles. The vessel is modeled assuming steel as the reference structural material, thus defining a conservative design scenario. The steel cost is calculated from the total mass of the cylindrical wall and the lids as:

$$C_{\mathrm{TES,st}} = b_{\mathrm{st}}\,\rho_{\mathrm{st}}\left(V_{\mathrm{TES,Wall,st}} + 2V_{\mathrm{TES,Lid,st}}\right) \tag{18}$$

where the structural volumes are defined as:

$$\begin{aligned} V_{\mathrm{TES,Wall,st}} &= \frac{\pi}{4}\left[\left(D_{\mathrm{TES}} + 2t_i + 2t_{\mathrm{st}}\right)^2 - \left(D_{\mathrm{TES}} + 2t_i\right)^2\right] L_{\mathrm{TES}} \\ V_{\mathrm{TES,Lid,st}} &= \frac{\pi}{4} D_{\mathrm{TES}}^2\, t_{\mathrm{st}} \end{aligned} \tag{19}$$

The steel wall thickness is determined by imposing mechanical resistance to the maximum operating pressure at the high-temperature side of the storage:

$$t_{st} = \frac{P_{PB}^{High}(D_{TES}+2t_i)}{2\left(\sigma_{st}-0.6P_{PB}^{High}\right)} \quad (20)$$

The solid storage material is treated separately, assuming the alumina cost to depend on the internal TES volume and the bed porosity:

$$C_{TES,S} = b_S\,\rho_S\,(1-\varepsilon)\,V_{TES} \quad (21)$$

The total TES cost is finally obtained as:

$$C_{TES} = N_{TES}\left(C_{TES,st}+C_{TES,S}\right) \quad (22)$$

This methodology ensures consistency between thermo-mechanical design and economic evaluation, providing a conservative estimate of the PBTES investment cost.

Gas system

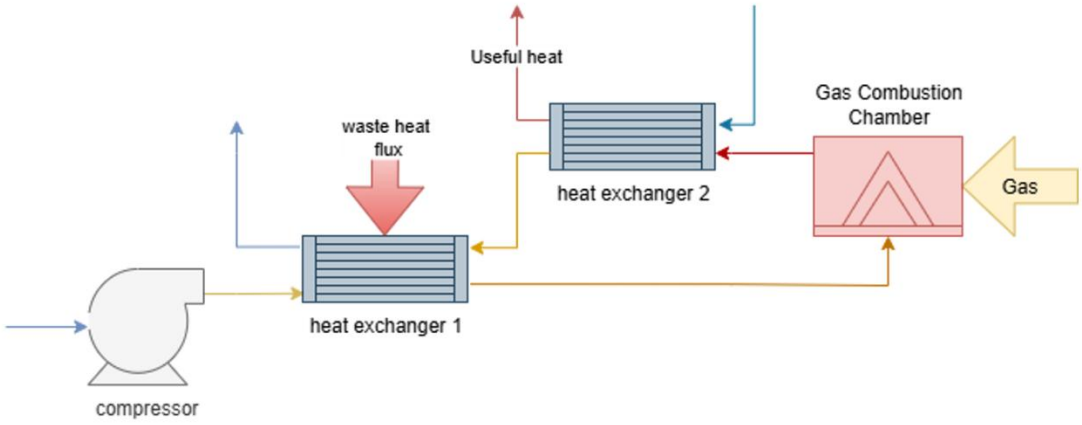

Figure 37 Complete gas-fired burner system

The gas-fired burner system (figure 37) adopted as a reference for the economic performance assessment is dimensioned using the same approach applied to the PBTES auxiliaries. Although industrial burners with comparable power ratings are already available on the market, they are not used as direct references, since industrial-scale equipment is typically sold through private negotiations and reliable price data are not publicly accessible. For this reason, the burner investment cost is estimated analytically using the correlation reported below:

$$Z_{CC} = \left(\frac{46.08\, \dot{m}_f}{0.995 - \frac{p_9}{p_7}} \right) [1 + \exp\left(0.018\, T_9 - 26.4\right)] \quad (23)$$

Both the investment costs have been fount summing the components cost and multiplying the result for a 1.5 factor, to ensure that the installation, logistics and connection between the components costs are covered.

2.2.2. Photovoltaic

The photovoltaic system considered in this research is a 1MWp solar farm, aimed to be coupled with the 100MWh PBTES to assure stability and energy dynamic management through the usage of low cost electricity during the day. The system has been located in Kongens Lyngby (Denmark), accurate climatic data are available in this area, in particular I used the PVGS [40] hourly irradiation data to estimate the electricity production of average commercial photovoltaic modules (21% efficiency). This electricity has been then used as input of the electric heater, and it has been prioritized respect to the energy purchase.

From the economic point of view, the investment cost for this PV system has been estimated at 780 000 €, from [41] the price in Denmark for a 1 MWp grid connected PV system is 4/7 dkk/Wp. this hypothesis permits to the system to be involved in the economic evaluation of the PBTES system investment.

2.2.3. Definition of the algorithm to buy electricity

The charging phase of the PBTES is planned on the day ahead energy market, available online from several private brokers and institutions [42] with good to excellent approximation, depending on several factors, well developed in [43]. the diagram in figure 38 shows the algorithm developed to purchase electricity at the lower price, through the day ahead prices data. The electricity buying functions follow three different curves (figure 39) used to effectively buy the electricity at a lower price and to use it as fuel for the PBTES charging. All are characterized by a monotonous decreasing dependency from the price, until a maximum price. This choice enables the formulation of a deterministic control strategy:

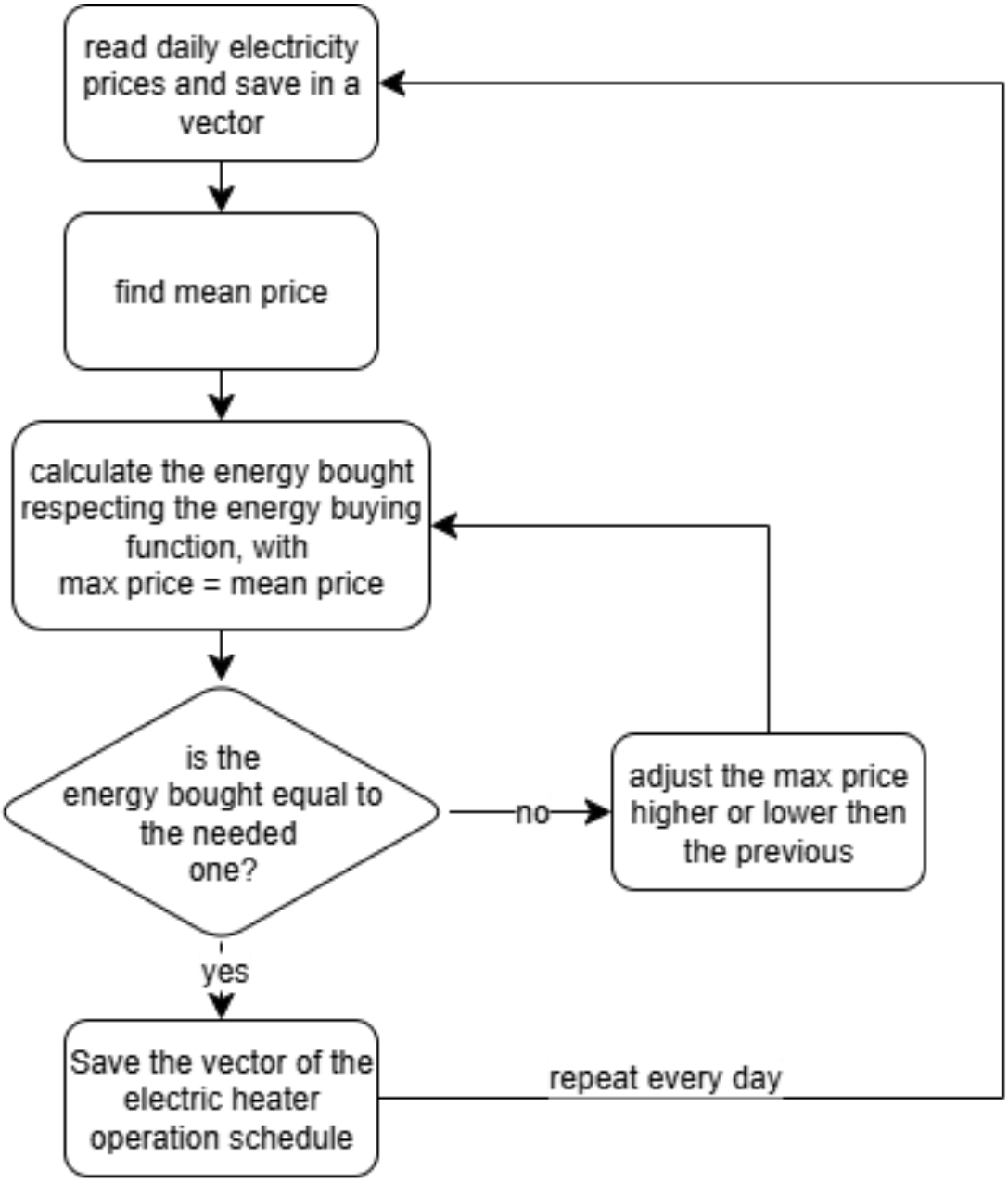

Figure 38 purchase algorithm

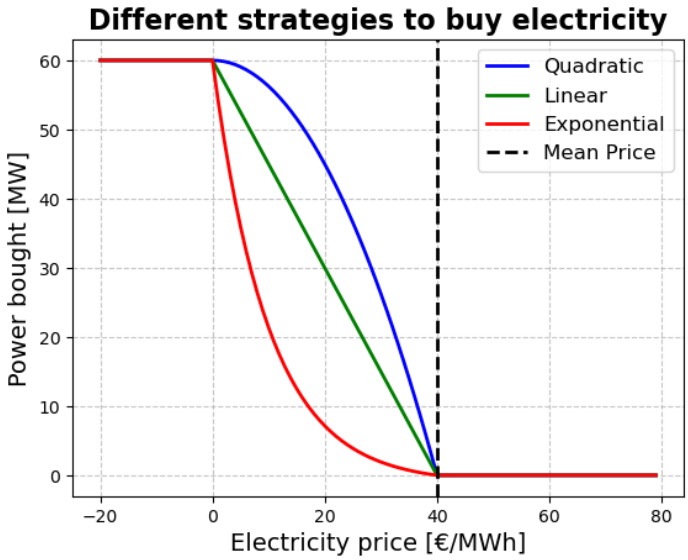

Figure 39 buying functions comparison

Starting from the electricity price vector, the average daily price is calculated, then, fixed the amount of energy needed to charge the TES in order to make possible a smooth and continuous energy supply to the user. Iteratively, the energy buying function is applied to the daily prices and the maximum amount of electricity buyable is found. Highest buying price is then adjusted to meet the need of energy, lowering or lifting it up. The buying schedule for the next day is so found, and it can be applied to a scheduled TES operation and not relying on real-time feedback.

This operation is applied separately to each day for all the simulated time so that the buying functions' performance are evaluated for different and realistic scenarios.

2.2.4. Real data origin

The technical-economic analysis of the PBTES system has been based on a data-based analysis conducted exclusively on real data, in order to guarantee operational consistency and to be representative of the market conditions. The input data include the electricity [44] and gas prices[45], disponible with hourly resolution until the day before of the analysis, considered from January 2015 to August 2025. These series have been used to evaluate the cost of the system, with reference to the gas-based reference, in different operational conditions.

The PV system production has been evaluated through photovoltaic historical data from the PVGS platform, selected for the simplicity, effectiveness and free availability, worldwide used for preliminary PV analysis. The timeseries covers the period from January 2015 to December 2023.

The totality of the external inputs on the system has been based on real data, ensuring a realistic behaviour and a solid base on the economical evaluation of the investment in the dynamic energy environment.

2.2.5. *Integration between the PBTES model, the electricity-buying algorithm, and the photovoltaic production.*

The integration between the charging algorithm and the physical model is linked thanks to the volumetric energy generation term of the heat equation of the solid phase and the velocity of the fluid.

The volumetric energy generation term $\ddot{\theta}$ is defined as:

$$\ddot{\boldsymbol{\theta}} = \frac{\boldsymbol{P}}{\boldsymbol{V_{beads}}} \tag{24}$$

The power P is the sum of the output of the electricity buying function and the PV farm power production. This term is controlled in real time, permitting to turn on just the section of the PBTES whose temperature is lower than the output's maximum acceptable one.

The power output is then computed through the formula:

$$\boldsymbol{P_{out}} = \dot{\boldsymbol{m}}\, \boldsymbol{c_{p,air}}\, (\boldsymbol{T_{max}} - \boldsymbol{T_0}) \tag{25}$$

Reversing it to find the air mass flow rate to send to the heat exchanger which will then "send" the energy to the user. Given the fixed power output hypotized in this study, and the almost constant output temperature, the air mass flow rate is considered constant.

The boundary conditions, this time are of imposed null flux at the first and last node, so adiabatic upper and lower plates:

$$\frac{\boldsymbol{dT}}{\boldsymbol{dz}} = \boldsymbol{0} \tag{26}$$

This condition, already applied in the validation phase to the upper plate, gave extremely good affinity with the experimental rig performance.

The integrated model has been evaluated through the *quality of the output* criteria, which permitted to calculate the performance, quantifying how much the system is capable to supply heat at a high enough temperature through an if condition in the code for every iteration, in which the output temperature is compared with the reference one. This criterion is the substitute of the operational efficiency, calculated as:

$$\eta = \frac{\int_0^t \dot{m} c_p (T(t) - T_0) dt}{\int_0^t \dot{m} c_p (T_{max} - T_0) dt} \quad (27)$$

Permits to calculate the performance on an extended period, not giving real time feedback on the operation, which is important given the dynamic behaviour of the system.

2.2.6. LCOE and NPV

The economic evaluation of the investment is conducted through two main indicators: the Net Present Value NPV and Levelized Cost Of Energy (or Heat, if we may further categorize the output energy type) LCOE/LCOH, both in discounted cost and in a investment period of 10 years, or 8 in the PV integrated version, this low amount of investment time is given by the limited real data available for free online. In this analysis NPV is not used as an indicator of the financial profitability based on cash flows, but as a measure of the total cost of the system during the whole life of the system. Consequently, NPV is defined as the sum of the initial CAPEX and the operative costs during the lifetime of the system, which are comprehensive of cost of electricity C_{energy} and maintenance costs OPEX, discounted through the discount rate $i = 5\%$:

$$NPV = CAPEX + \sum_{y=0}^{YEARS} \frac{OPEX + C_{energy}}{(1+i)^y} \quad (28)$$

In this formula, NPV results in a value higher than zero and increases with the time, because it represents the accumulation of the overall costs of the system, it does not include earnings but compares several types of investments aimed to the construction and operation of heat production systems for the industrial user.

LCOE is calculated as the ratio between the total actualized cost of the energy, calculated exactly like in the NPV and the useful energy supplied to the user during the operational lifetime.

$$LCOE = \frac{CAPEX + \sum_{y=0}^{YEARS} \frac{OPEX + C_{energy}}{(1+i)^y}}{\sum_{y=0}^{YEARS} \frac{Energy_{used}}{(1+i)^y}} \quad (29)$$

The energy $Energy_{used}$ is hypotized from a constant power output of 7 MW since the brillant results obtained in the quality of energy that will be shown in Chapter 2.3.4

Both the indicators have been confronted to the ones calculated for the reference gas system. Modeled for the same investment time and discount rate. The confrontation in the NPV and LCOE allows assessing if the adoption of PBTES leads to a reduction in the total discounted cost and/or in the specific cost of the delivered energy compared to the conventional solution, thus providing a quantitative criterion to evaluate the investment feasibility.

2.3. Results

2.3.1. Auxiliary Components Sizing Results

This section presents the results obtained from the sizing methodology applied to the auxiliary components of the system, the air compressor and the heat exchangers.

Figure 40 shows the sizing outcome for the compressor, where the electrical power requirement is reported as a function of the number of compression stages. As the number of stages increases, the required electrical power decreases, reflecting the reduction in specific compression work associated with a lower pressure ratio per stage. The estimated compressor cost exhibits an increasing trend with increasing stages of 15-20% per stage [46].

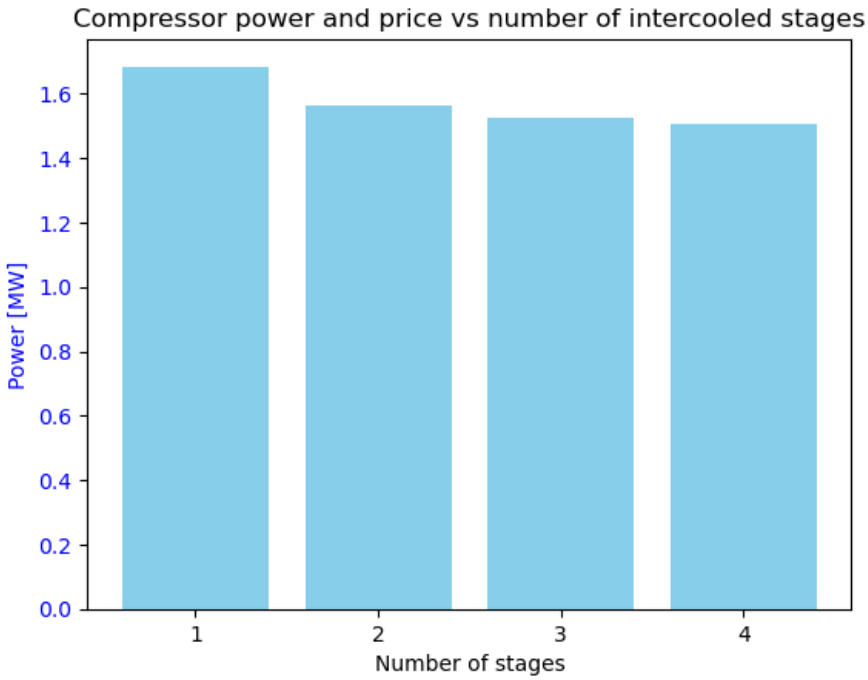

Figure 40 Compressor power varying the number of stages

The increase in the price of the compressor given by the addiction of several stages do not justify the choice of a multistage compressor given the relatively small gain in power savings and the increase on the maintenance cost.

The cost of the single stage compressor is 223000 €, based on the formula (11).

The sizing procedure was applied consistently to the heat exchangers integrated within the system. Based on the same thermodynamic boundary conditions and design constraints, the resulting estimated investment costs are:

- Heat Exchanger 1 (HX1): 103867 €
- Heat Exchanger 2 (HX2): 30900 €

These values are obtained from the geometrical and thermal sizing methodology previously described and are reported here as direct outputs of the component-level design process.

The PBTES, whose walls are made of Stainless Steel 310, with magnetite beads, has a cost of 980 000 €.

2.3.2. Electricity Purchasing Algorithm Results

This section presents the results obtained from the application of the electricity purchasing algorithm to the system operation. Among the different strategies investigated during the analysis, only the quadratic method is reported here, as illustrated in figure 41, which is representative of the overall behaviour observed across the full set of analysed cases.

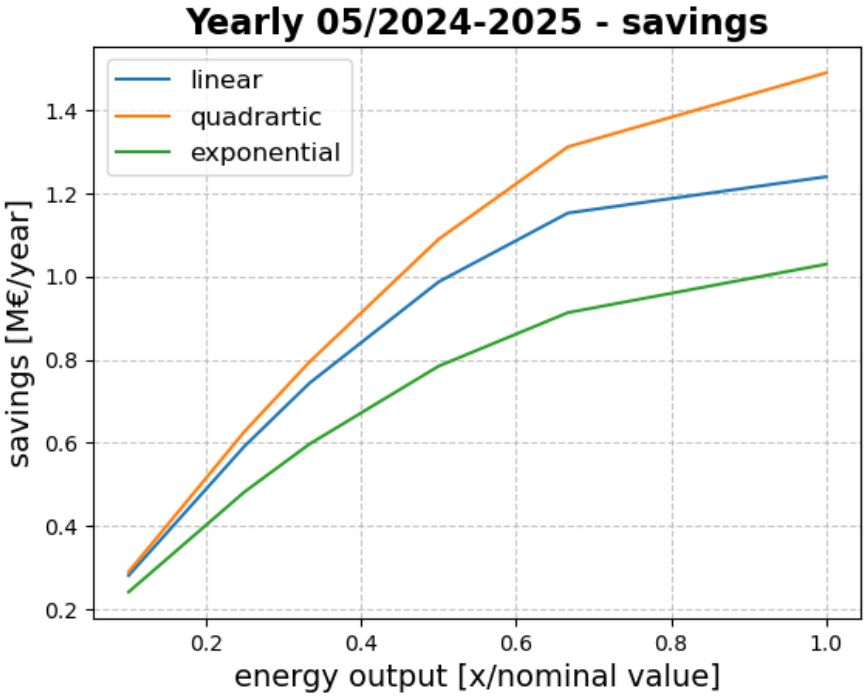

Figure 41 savings in a year period varying energy output for different buying functions

Four figures are presented to describe the economic performance of the algorithm. Two figures report the annual electricity cost (figure 42) and the corresponding annual savings (figure 43), defined relative to a reference case in which electricity is purchased instantaneously at the market price without any optimization strategy. The graph has been obtained for different power outputs of the PBTES system, from 1/10th to the nominal 20 MW, highlighting how the power needed from the user changes the investment evolution.

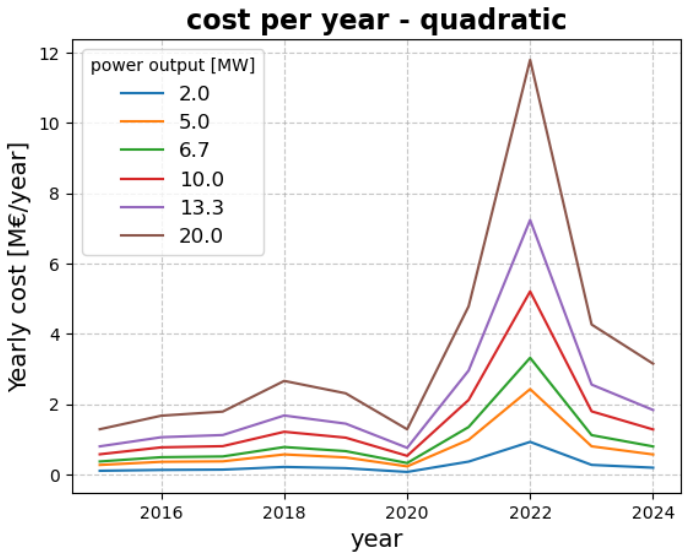

Figure 42 Yearly electricicy cost for every year of simulation for different output powers

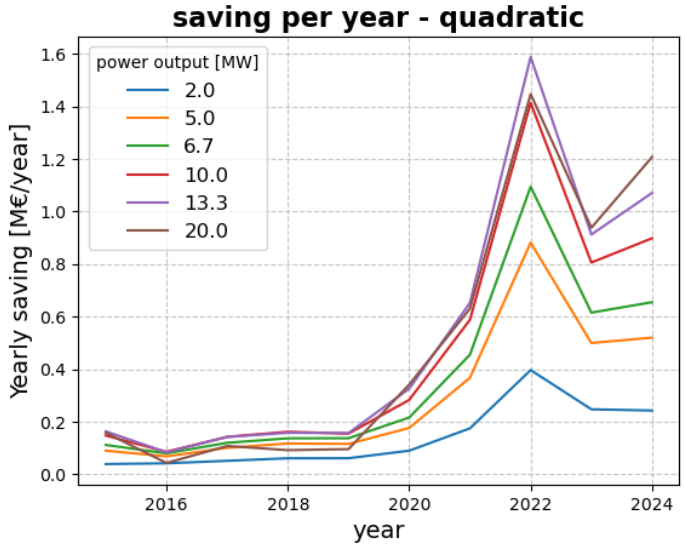

Figure 43 Yearly savings for every year of simulation for different output powers

The remaining two figures show the cumulative electricity cost and the cumulative savings, calculated year by year over the considered time horizon through the progressive sum of the costs, for the N^{th} year the corresponding cost value is:

$$C_N = \sum_{i}^{N} c_i \tag{30}$$

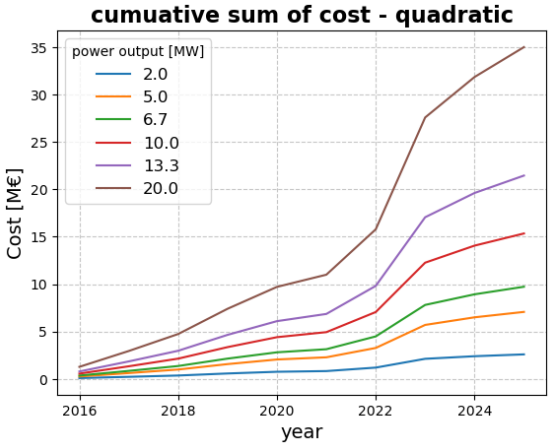

Figure 44 Cumulative cost of electricity for every year of simulation for different output powers

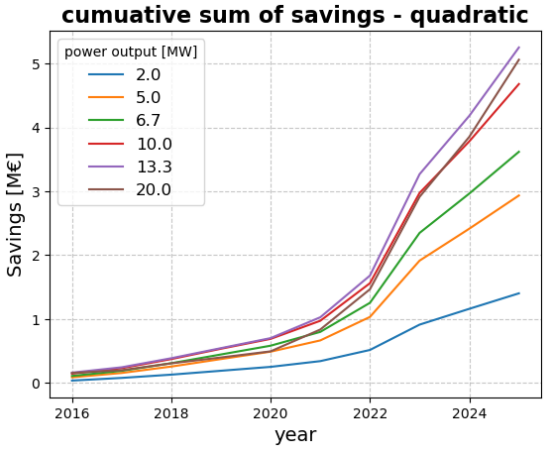

Figure 45 Cumulative saving for every year of simulation for different output powers

2.3.3. Integration of photovoltaic

The same analysis has been carried out also for the PV integrated scenario. The four following figures (figure 46-49) show the results of the analysis, the explanation of the graphs in Chapter 2.3.2 reflects also the following figures which do not differ in methodology but just on the combined input of electricity in the system.

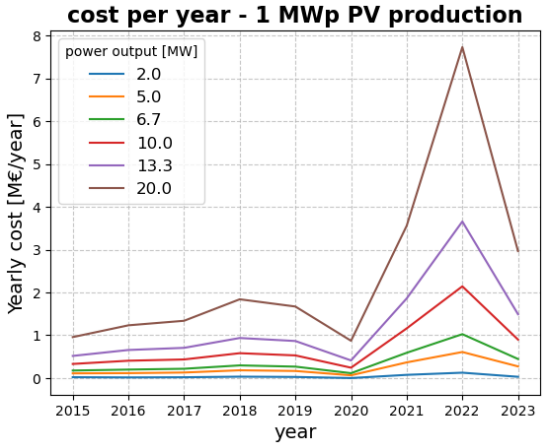

Figure 46 Yearly electricicy cost for every year of simulation for different output powers – PV integrated system

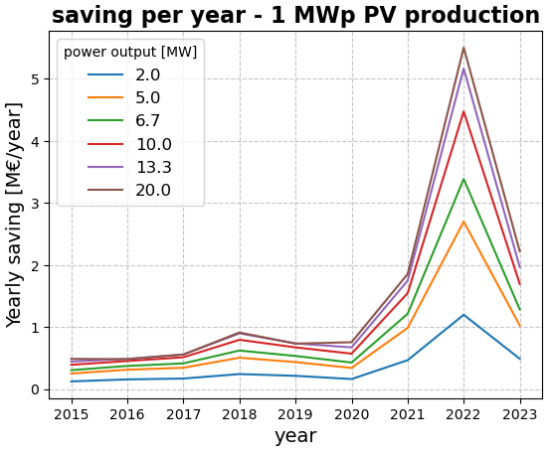

Figure 47 Savings for every year of simulation for different output powers – PV integrated system

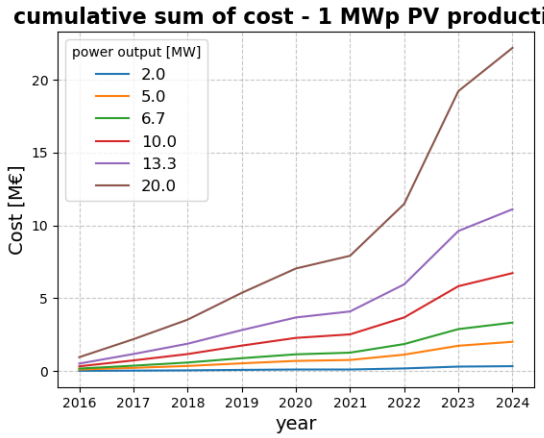

Figure 48 Cumulative cost of electricity for every year of simulation for different output powers – PV integrated system

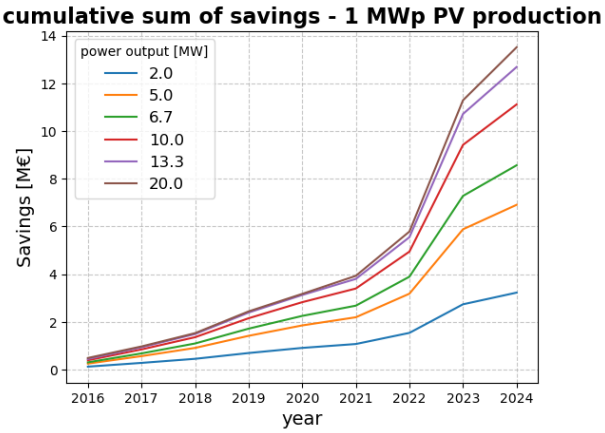

Figure 49 Cumulative saving for every year of simulation for different output powers – PV integrated system

2.3.4. Application of the buying algorithm to the physical model

The vector resulting from the electricity buying function is then used as input in the electric charging system as in chapter 2.2.5. The performance of the system is influenced by the uneven charging of the PBTES, conditioned by the energy price variation. The following graphs are the results of the simulation of an almost 10 years simulation (Jan 2015 – Aug 2025), the quality of the output in percentage of time over the total amount of simulation hours is plotted in two different scenarios.

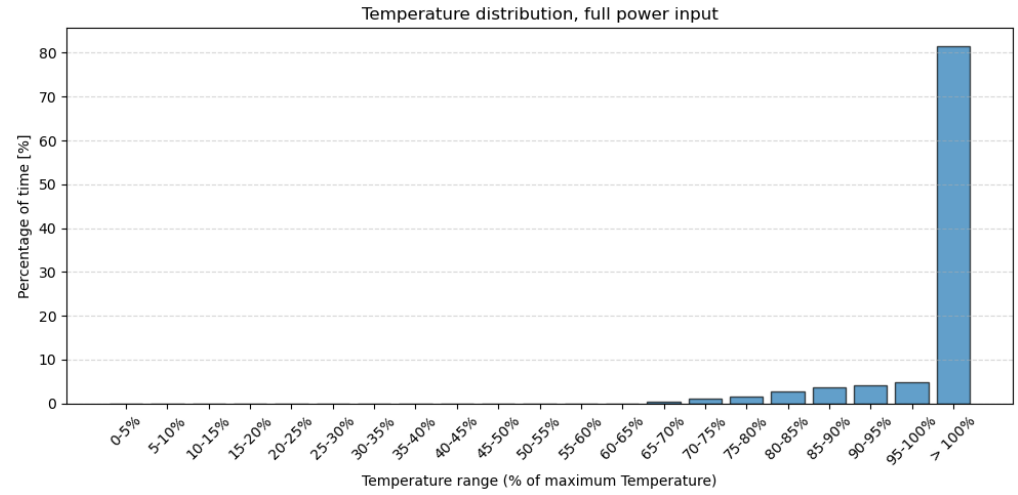

Figure 50 Temperature of the output mass flow rate – full power input

Figure 50 shows the output of a simulation with a full amount of electricity output (7 MW max input), figure 51 shows the results if the electricity output is limited to max 2/3 of the full amount (~5 MW). It is worth clarifying that the simulations with or without the PV integration are thermodynamically identical, the only difference being economic, this because even under peak production conditions, the PV system (1 MW) can supply only a small fraction of the electric heater demand (20 MW) As a result, the electricity generated by the PV system is never sufficient to exceed either the heater power demand or the daily energy requirement, but only serves to reduce the amount of electricity purchased from the grid, and does not affect the quality of the thermal output, whose trend remains unchanged.

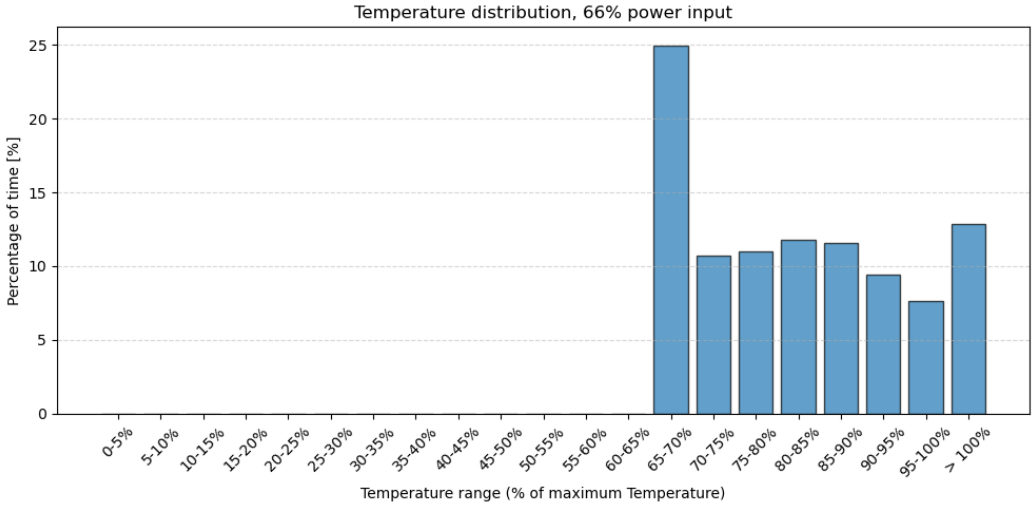

Figure 51 Temperature of the output mass flow rate – two thirds of nominal input

2.3.5. Net Present Value and LCOS

The economic results are reported for the complete set of system configurations analyzed over the full-time horizon covered by the input datasets. The considered scenarios include

the PBTES system operated with optimized electricity purchasing without photovoltaic integration and with photovoltaic integration, as well as two reference cases: a gas-fired thermal system and a configuration based on instantaneous, unoptimized electricity purchases from the electricity market. All scenarios are evaluated over aligned calendar years and under identical economic assumptions, ensuring consistency in the comparison of the reported results.

The Net Present Value (NPV) (figure 52) results are presented as a function of calendar year, showing the cumulative discounted economic outcome for each analysed scenario. Each curve reflects the progressive accumulation of discounted cash flows over time, accounting for the specific cost structure associated with each configuration and allows tracking the temporal evolution of the economic performance across the full duration of the analysed period.

It is well visible that at the start of the timetable, the CAPEX of the gas-based system is negligible with respect of the PBTES ones, but after 9 years, the investment of the PV integrated PBTES system is just 22% higher than the gas based one. This difference tends to be always smaller with the time.

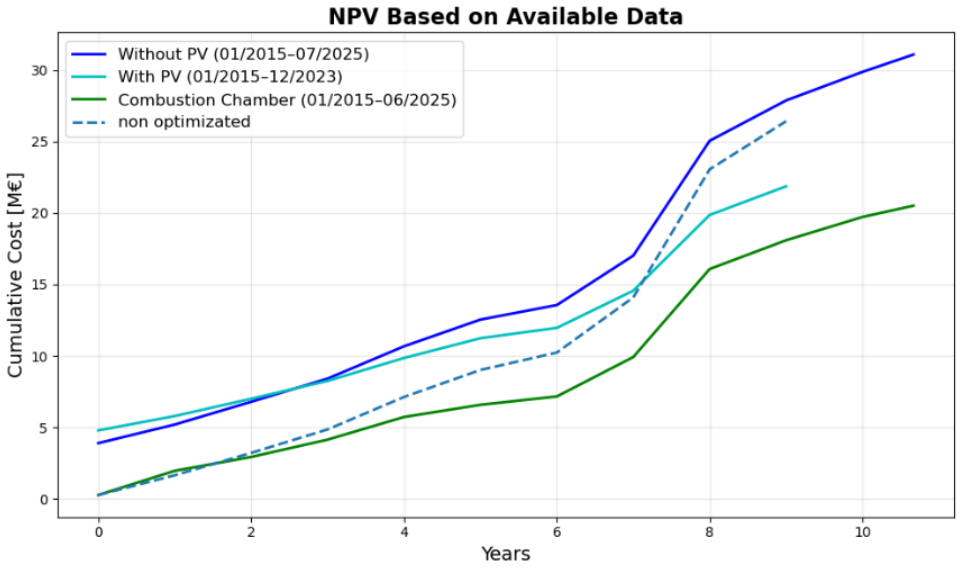

Figure 52 NPV of the different kinds of system examined

The Levelized Cost of Energy (LCOE) (figure 53) results are reported for the same set of scenarios, expressed as a time-dependent metric over the considered calendar years. The LCOE curves show the evolution of the discounted average cost per unit of delivered energy as costs and useful energy are accumulated over time. The storage-based configurations with and without photovoltaic integration are reported alongside the gas-

based reference system, allowing a consistent visualization of cost-normalized performance; the mean electricity price per year is also plotted as reference.

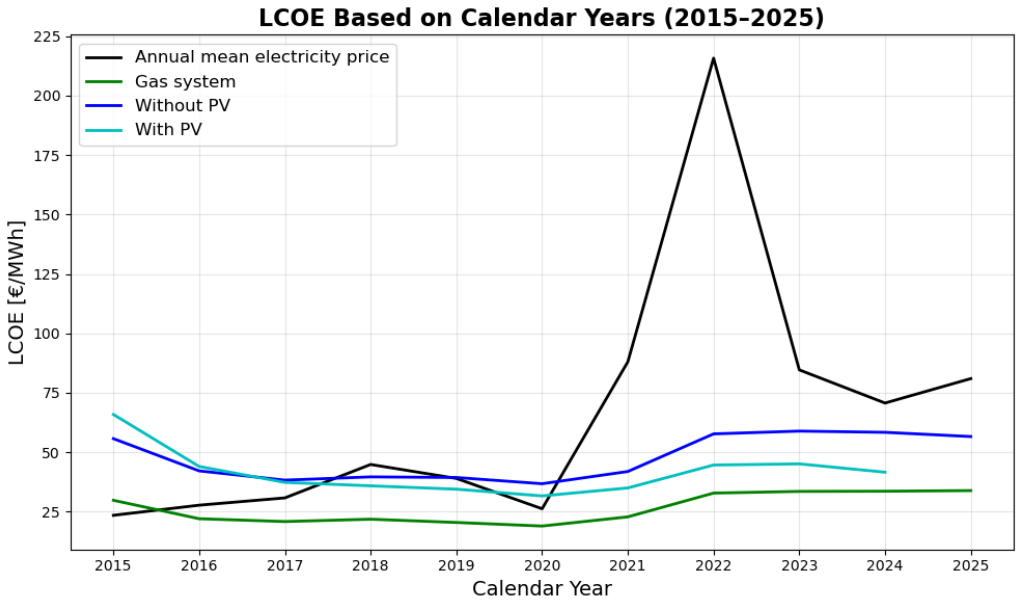

Figure 53 Levelized Cost of Energy for the differnet kinds of systems examined

2.4. Conclusions

2.4.1. The system price

The total cost of the PBTES system, including the two heat exchangers, the compressor, the storage tank, and the solid filler material (beads), has been estimated at €2,002,000.

Following the same logic the gas system cost is 386 400 €.

2.4.2. How the changings in the inlet electric power, changes the cost and savings

The electric heater has a maximum power inlet, because it has been modeled on a real one, this limits the amount of power that can be bought instantaneously. If we vary the outlet air mass flow rate, so the outlet power of the system, a different amount of time will be needed to fully charge the PBTES. This changes the cost and savings connected with the electricity buying algorithm.

There is an optimized value for our kind of system that assures maximum savings. This behaviour is well shown in the savings plot (figure 45) where the savings of the 3 higher output values are comparable, even if the highest one is 20 MW and the 3rd is 10 MW. This

because given a fixed electricity inlet of the heater, I will raise the savings until a maximum value, that will then lower again when the power output is high enough to make the algorithm buy electricity at higher prices.

In the PV integrated scenario (figure 47) the bought electricity is lower thanks to the auto consumption. This makes the maximum saving level to be shifted to the higher end. It is reasonable, based on the data that there will be a crossover point where the PBTES and gas system investment profiles will converge; beyond that point, PBTES will outperform the gas based system, within the lifespan of the PBTES system.

The comparison between the RES integrated model and the one fully charged by the grid highlights a total saving of more than 180% more for the photovoltaic integrated model. Over 14 M€ against 5 M€ in savings gained in 10 years of life of a full scale PBTES, with a ~800 000 € investment.

The proposed method is explicitly based on the energy demand of the PBTES: by iterating the day-ahead price threshold, it ensures each day the amount of electrical energy required to charge the TES up to the target thermal level, thereby optimizing the quality of the storage output in terms of energy availability and stability of the heated air mass flow rate at the outlet. This approach avoids situations in which the TES is only partially charged for economic reasons, resulting in a reduction of the stored thermal energy and potential losses in the operational efficiency of the system.

In the literature, alternative approaches based on real-time pricing and adaptive control for energy systems with storage have been explored, making use of advanced forecasting techniques and machine learning to dynamically update operational decisions; however, such approaches require complex statistical models and a significant increase in computational and control complexity. In the case of a PBTES, a charging strategy driven exclusively by instantaneous price signals could lead to incomplete charging of the storage system, with negative effects on the quality of the heat delivery profile and on the outlet air mass flow rate. Future studies could nonetheless further investigate the applicability of real-time control strategies based on machine learning and stochastic optimization methods, assessing their specific benefits and drawbacks in the context of PBTES systems.

From the *Quality of the output* section, we can deduct that in our case, an under dimensioned inlet electric heater leads to a highly lower quality in the output which contrasts with our initial hypothesis: an output mass flow rate at stable temperature. I chose to continue with a non-scaled energy input to contrast the losses in performance and grant an optimal output during the most hours. The fully scaled PBTES grants an air mass flow rate temperature over the nominal T_{max} for over 80% of the time and an output with 15% of tolerance for the 95% of the time.

2.4.3. NPV and LCOE comments, discussion on the projections of the prices on future.

In our case it is not correct to talk about a Levelized Cost Of Storage LCOS, because the main objective of the PBTES is not anymore to store for long time (more appropriate for long-mid term operation), but to buy energy from the grid day by day, the main objective of the system is to provide continuously cheap electricity, so LCOE is the right parameter to observe.

The PBTES system is compared with a gas-powered system for the economic analysis, which stands for its low cost and good return on the investment, especially in the short term. However, in the NPV graph we can see that the PV integrated system, shortens its distance with the gas-powered systems especially in the second half, we can forecast optimistically an overtake of the studied system in the following 3 to 6 years.

The effects of the COVID-19 pandemic and of the Russian gas crisis starting in 2021 are clearly visible in the data-based Net Present Value trends. These events led to unprecedented volatility and sustained increases in energy prices, which strongly affected the economic performance of energy-intensive industrial processes. In this context, energy independence has become a central strategic issue for industrial stakeholders.

The results show that the adoption of innovative energy technologies combined with renewable energy sources can significantly mitigate the exposure of industrial systems to external shocks in international energy markets. Even though renewable generation is intrinsically intermittent, its integration with thermal energy storage systems allows decoupling energy procurement from energy use, thereby reducing sensitivity to short-term price spikes and geopolitical instability. Consequently, such solutions enable substantial cost savings over the project lifetime while lowering the dependence of industrial operations on international relations and fossil fuel supply chains, ultimately enhancing both economic resilience and long-term competitiveness.

The proof of this is shown in regular shape of the figure 42 - 43 – 46 – 47 until 2020, which is interrupted by the year 2021-2024 part, the graphs are presenting the price spent to buy electricity and savings achieved using the analyzed system. The right part of the graph is characterized by a price more than five times higher than the average, this is because of the correlation between electricity and gas prices, highly influenced by the geopolitical situation of Russia in that period, which is a main exporter of gas and influences the gas price also for countries which produce their own gas or do not buy gas from Russia as Denmark. And this is well noticeable in the previously mentioned figures as well as in the

energy price line (black) in figure 53. Figure 54 also shows that rom 2020 to 2023 Covid reduced the internal production of gas, resulting in a net balance shifted on the imports for the first time in recent years.

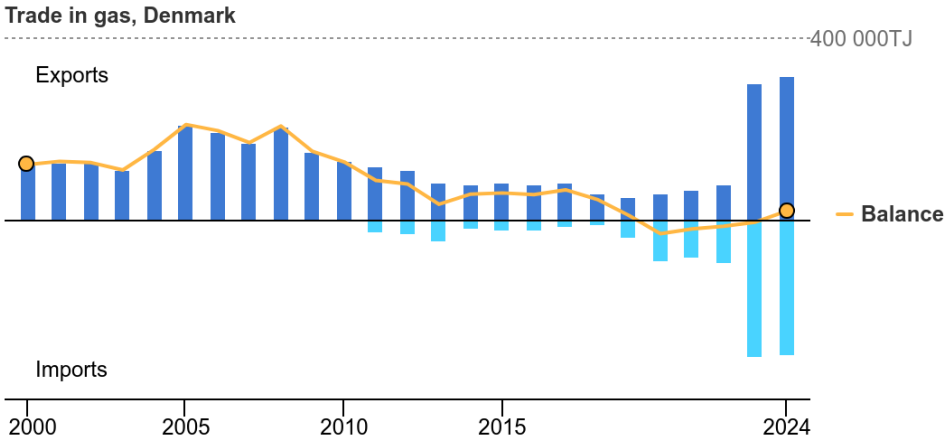

Figure 54 gas import and export of Denmark

This analysis is limited to publicly available data obtained from online sources. The forecasting of energy prices is a highly complex topic that requires substantial analytical effort and is often affected by significant uncertainty, leading to limited accuracy in long-term predictions. For this reason, the present study deliberately relies on historical price data, allowing the analysis to remain grounded in real and verifiable market conditions while ensuring internal consistency and robustness of the economic assessment.

Chapter 3: RQ3 and discussion of the results

3.1. About the research

How does the implementation of a dynamic behaviour on a PBTES improve the resilience and flexibility of the electricity and district heating grid? Is this method a valid support for the decarbonization of the hard-to-abate industrial sector?

The implementation of a dynamic operating strategy for a PBTES system directly addresses the increasing stability and reliability challenges faced by electricity grids with a high penetration of renewable energy sources. In several countries, and potentially also in more developed grids, the further deployment of variable renewable generation is expected to exacerbate peak load issues and periods of over-generation, particularly from wind power. In this context, the large-scale adoption of electrically charged PBTES systems represents a viable solution to mitigate peak demand and to absorb excess

renewable electricity that would otherwise be curtailed.

At the same time, a higher share of renewables in the energy mix leads to a reduction in the operation of cogeneration plants, resulting in a lower availability of large-scale thermal power for district heating networks. Consequently, district heating systems require alternative heat sources. The proposed system generates more than 10 kg/s of air at approximately 100 °C as waste heat, which can be effectively utilized for third- and fourth-generation district heating networks, characterized by supply temperatures below 100 °C.
The adoption of cross-flow heat exchangers allows the air to exit the system at 2.4 bar, enabling direct coupling with additional heat exchangers or, in the case of clean air rather than industrial exhaust gases, further compression and direct injection into the district heating network. This configuration can be achieved through a single-stage compressor with a compression ratio of 3, increasing the downstream air temperature to 390 K and raising the outlet temperature of the first heat exchanger above 100 °C, with an associated investment cost of 16,000 €.

In parallel, the decarbonization of heavy industry remains a critical challenge, as this sector is responsible for a significant share of global emissions. Most high-temperature industrial processes currently rely on fossil-fuel-based systems, such as gas turbines, diesel engines, and coal-fired units. The electrification of these processes, combined with the optimization and recovery of waste heat, represents a transformative shift for the industrial sector.
Even when electricity is supplied by fossil-based utility-scale power plants, the higher efficiency of large and centralized units compared to industrial-scale generators leads to reduced fuel consumption and lower overall emissions.

Finally, the combined deployment of renewable energy sources and energy storage contributes to a more predictable energy market, reducing exposure to geopolitical dynamics and international relations. Energy prices are strongly influenced by a limited number of fossil fuel producers, whose supply decisions have a direct impact on electricity and heat generation in dependent countries, as demonstrated by the reduction in Russian gas supplies to Europe in the second half of 2021. Renewable energy offers a pathway to decentralize this influence, but effective alternatives to fossil fuels require the integration of storage technologies.
In this context, a dynamically operated PBTES system can play a central role, supporting both medium- and high-temperature industrial processes in hard-to-abate sectors and the evolution of modern district heating networks.

3.2. About the models

The integration of the PBTES numerical model with the electricity purchasing algorithm results in a complex yet highly adaptable framework, suitable for different grid configurations and industrial applications, while maintaining a robust and consistent structure.

Talking about the electricity purchasing algorithm, the same analytical framework can be readily applied to different geographical contexts by modifying the underlying energy mix, including electricity purchasing patterns and the renewable generation mix, as well as by adapting the market data to different zones. This may lead to different quantitative outcomes without altering the core modelling approach. In general, this class of systems tends to achieve higher performance in electricity markets that are less centrally controlled, more exposed to renewable generation, and characterized by a liberalized price formation mechanism, where variability and price signals can be effectively exploited by a dynamically operated storage system. The preservation of the same coupling between the electricity market, the charging strategy, and the detailed thermal model ensures methodological robustness and allows meaningful comparisons across different scenarios.

The thermodynamic model of the PBTES is fully scalable and adaptable to different types of industrial users. The system can be dimensioned to match a wide range of plant sizes, to deliver the required output temperature, and to recycle different waste heat streams allowing its application to industrial processes with heterogeneous thermal demands. This flexibility directly supports the objectives of the present research, as it enables the assessment of how a dynamically operated PBTES can enhance resilience and flexibility not only at the level of a single case study, but at the broader system scale, encompassing both electricity grids and thermal energy users in hard-to-abate industrial sectors.

Conclusion

The decarbonization of high temperature industrial processes is one of the most critical focusses of the energy transition, due to strong dependence on fossil fuels. Electrification offers a viable pathway, but its effectiveness is limited by the variability and cost of electricity. The study is framed within a highly renewable and liberalized electricity system, such as the Danish market, where price formation is strongly influenced by intermittent renewable generation. The increasing occurrence of low and negative price periods, combined with high price volatility, creates both challenges and opportunities for industrial energy users. However, the demand for reliable and high temperature heat of the industrial users cannot depend on the unstable prices of electricity.

Within this context this research has analysed the potential of PBTES as an enabling technology for electrification of industrial processes, proposing a change in the conception of TESs: from passive storage systems to an active and flexible component of the industrial facility, allowing industrial processes to exploit electricity market dynamics while ensuring a stable and efficient thermal energy supply. By coupling energy storage with data-driven operation strategies, the system aims to transform price variability from a constraint into a resource, supporting both industrial decarbonization and energy system flexibility.

The work has been structured combining thermofluid dynamics modelling, system design, and techno-economic evaluation.

Firstly, developing and validating a numerical model based on a one-dimensional two-phase design. The model has been used to investigate different operating regimes, including long-term, short-term, and dynamic operation, and to assess the influence of design parameters such as geometry, material properties, and operational constraints, finding a suitable configuration to be used in dynamic operation.

The integration of the system in an industrial context has been carried out through a data-based analysis relying on real electricity and gas price datasets over multiple years. A dedicated algorithm has been developed to exploit price variability, enabling the simulation of realistic operating strategies and their impact on both system performance and economic outcomes.

The economic evaluation has then been conducted by embedding the PBTES within a complete system specifically designed for industrial operation and waste heat recovery. In this configuration, the storage is not treated as a stand-alone component, but as part of an integrated system including auxiliary components such as compressors, heat

exchangers, and an electric heating unit, all interacting to ensure reliable and continuous delivery of high-temperature heat. The analysis accounts for both capital and operational expenditures, linking the thermodynamic performance of the system to its economic viability.

Furthermore, the integration of waste heat streams and local renewable generation has been considered within the modelling framework, in order to assess their role in shaping the operation and the economic behaviour of the system. This approach provides a consistent basis for the comparative evaluation of the PBTES solution against conventional alternatives.

The sizing of the PBTES resulted in the usage of a single tank of 700 m^3 because of the gain in performance given by the volume increase, filled with 8 mm beads of magnetite., to ensure a good compromise between pressure losses and heat exchange surface between the medias; the magnetite is one of the most used in the recent PBTES systems and the numerical analysis enlightened the reason of this choice. The aspect ratio (height over diameter ratio) has been fixed to 3.

The results demonstrate that the value of PBTES is determined by its thermodynamic performance as storage, already demonstrated in many studies, and its ability to operate dynamically within a volatile energy system. While conventional seasonal operation leads to energy losses and limited efficiency, and cyclic operation achieves high efficiency at the cost of low utilization (around 30%), the dynamic approach enables a more effective exploitation of the storage capacity. The system proves capable of satisfying industrial temperature requirements for more than 98% of the operating time, ensuring a high level of reliability when examined under realistic conditions, based on the real data of electricity prices together with the algorithm developed for its electricity purchase.

The system provided performance comparable with a gas system with a higher upfront investment of approximately 22% compared to it, the overall framework highlights the potential of PBTES as a competitive and flexible solution for industrial energy supply.

Beyond the specific results obtained in this work, the most relevant outcome comes from the wide applicability of the analyzed PBTES system. It does not represent a simple energy storage but a real flexible energy interphase that can connect electricity heat and industrial processes. Transforming the discontinuity between demand and production of heat in a solved problem. In this perspective the PBTES can be integrated in energy hubs and industrial clusters, where it is ready to absorb renewable surplus, recover waste heat and redistribute thermal energy, becoming a central node in circular energy systems.

In the same way, the model developed can enables going beyond a simple description of the system, giving the possibility to implement advanced control strategies based on real data, real time optimization and predictive approaches. The integration with the external signals makes possible a smart and adaptable management of energy over time.

As a result, Both the system and the model emerge as enabling tools for a more advanced energy management. In a context which is increasingly decentralized, digital and interconnected, the PBTES does not only store energy, but contributes actively to shape its utilization, positioning itself as a key component of a flexible, resilient and sustainable system.

Bibliography

[1] 'Immagazzinamento dell'energia', *Wikipedia*. Mar. 13, 2025. Accessed: Apr. 01, 2025. [Online]. Available: https://it.wikipedia.org/w/index.php?title=Immagazzinamento_dell%27energia&oldid=144001588

[2] C. A. Wankouo Ngouleu, Y. W. Koholé, F. C. V. Fohagui, and G. Tchuen, 'Optimum design and scheduling strategy of an off-grid hybrid photovoltaic-wind-diesel system with an electrochemical, mechanical, chemical and thermal energy storage systems: A comparative scrutiny', *Applied Energy*, vol. 377, p. 124646, Jan. 2025, doi: 10.1016/j.apenergy.2024.124646.

[3] A. Benato and A. Stoppato, 'Pumped Thermal Electricity Storage: A technology overview', *Thermal Science and Engineering Progress*, vol. 6, pp. 301–315, Jun. 2018, doi: 10.1016/j.tsep.2018.01.017.

[4] P. Schwarzmayr, F. Birkelbach, H. Walter, and R. Hofmann, 'Standby efficiency and thermocline degradation of a packed bed thermal energy storage: An experimental study', *Applied Energy*, vol. 337, p. 120917, May 2023, doi: 10.1016/j.apenergy.2023.120917.

[5] H. Jouhara, A. Żabnieńska-Góra, N. Khordehgah, D. Ahmad, and T. Lipinski, 'Latent thermal energy storage technologies and applications: A review', *International Journal of Thermofluids*, vol. 5–6, p. 100039, Aug. 2020, doi: 10.1016/j.ijft.2020.100039.

[6] E. Weise, 'Liberalisation of the Danish power sector, 1995-2020'.

[7] 'Frontpage', GreenLab. Accessed: Apr. 25, 2025. [Online]. Available: http://www.greenlab.dk/

[8] D. A. Elalfy, E. Gouda, M. F. Kotb, V. Bureš, and B. E. Sedhom, 'Comprehensive review of energy storage systems technologies, objectives, challenges, and future trends', *Energy Strategy Reviews*, vol. 54, p. 101482, Jul. 2024, doi: 10.1016/j.esr.2024.101482.

[9] M. Cascetta, F. Licheri, R. P. Merchán, and M. Petrollese, 'Operating performance of a Joule-Brayton pumped thermal energy storage system integrated with a concentrated solar power plant', *Journal of Energy Storage*, vol. 73, p. 108865, Dec. 2023, doi: 10.1016/j.est.2023.108865.

[10] N. Georgousis, J. Diriken, M. Speetjens, and C. Rindt, 'Comprehensive review on packed-bed sensible heat storage systems', *Journal of Energy Storage*, vol. 121, p. 116516, Jun. 2025, doi: 10.1016/j.est.2025.116516.

[11] ‘Rondo Energy’. Accessed: Nov. 05, 2025. [Online]. Available: https://www.rondo.com/

[12] J. D. McTigue, A. J. White, and C. N. Markides, ‘Parametric studies and optimisation of pumped thermal electricity storage’, *Applied Energy*, vol. 137, pp. 800–811, Jan. 2015, doi: 10.1016/j.apenergy.2014.08.039.

[13] L. Geissbühler *et al.*, ‘Pilot-scale demonstration of advanced adiabatic compressed air energy storage, Part 1: Plant description and tests with sensible thermal-energy storage’, *Journal of Energy Storage*, vol. 17, pp. 129–139, Jun. 2018, doi: 10.1016/j.est.2018.02.004.

[14] ‘World’s largest thermal energy storage unit inaugurated by Kyoto Group at KALL Ingredients in Hungary’. Accessed: Mar. 04, 2026. [Online]. Available: https://www.kyotogroup.no/news/worlds-largest-thermal-energy-storage-unit-inaugurated

[15] R. Tiskatine *et al.*, ‘Suitability and characteristics of rocks for sensible heat storage in CSP plants’, *Solar Energy Materials and Solar Cells*, vol. 169, pp. 245–257, Sep. 2017, doi: 10.1016/j.solmat.2017.05.033.

[16] D. Pérez-Gallego, J. Gonzalez-Ayala, A. Medina, and A. Calvo Hernández, ‘Comprehensive review of dynamical simulation models of packed-bed systems for thermal energy storage applications in renewable power production’, *Heliyon*, vol. 11, no. 4, p. e42803, Feb. 2025, doi: 10.1016/j.heliyon.2025.e42803.

[17] B. Koçak, M. Majó, C. Barreneche, A. I. Fernández, and H. Paksoy, ‘Performance analysis of a molten salt packed-bed thermal energy storage system using three different waste materials’, *Solar Energy Materials and Solar Cells*, vol. 278, p. 113199, Dec. 2024, doi: 10.1016/j.solmat.2024.113199.

[18] T. Nahhas, X. Py, and R. Olives, ‘Life Cycle Assessment of Air-Rock Packed Bed Storage System and Its Comparison with Other Available Storage Technologies for Concentrating Solar Power Plants’, *Waste Biomass Valor*, vol. 11, no. 5, pp. 2357–2365, May 2020, doi: 10.1007/s12649-018-0529-x.

[19] E. Oró, A. Gil, A. de Gracia, D. Boer, and L. F. Cabeza, ‘Comparative life cycle assessment of thermal energy storage systems for solar power plants’, *Renewable Energy*, vol. 44, pp. 166–173, Aug. 2012, doi: 10.1016/j.renene.2012.01.008.

[20] M. Cascetta, G. Cau, P. Puddu, and F. Serra, ‘Numerical Investigation of a Packed Bed Thermal Energy Storage System with Different Heat Transfer Fluids’, *Energy Procedia*, vol. 45, pp. 598–607, Jan. 2014, doi: 10.1016/j.egypro.2014.01.064.

[21] T. Esence, A. Bruch, S. Molina, B. Stutz, and J.-F. Fourmigué, 'A review on experience feedback and numerical modeling of packed-bed thermal energy storage systems', *Solar Energy*, vol. 153, pp. 628–654, Sep. 2017, doi: 10.1016/j.solener.2017.03.032.

[22] 'Hallet, R.W. Jr., Gervais, R.L., 1977. Central receiver solar thermal power system – Phase 1 - CDRL ITEM 2 - Pilot Plant Preliminary Design Report - Vol V - Thermal Storage Subsystem, SAN/1108-8/5.'.

[23] J. E. Pacheco, S. K. Showalter, and W. J. Kolb, 'Development of a molten-salt thermocline thermal storage system for parabolic trough plants', *Journal of Solar Energy Engineering, Transactions of the ASME*, vol. 124, no. 2, pp. 153–159, 2002, doi: 10.1115/1.1464123.

[24] G. Zanganeh, A. Pedretti, S. Zavattoni, M. Barbato, and A. Steinfeld, 'Packed-bed thermal storage for concentrated solar power – Pilot-scale demonstration and industrial-scale design', *Solar Energy*, vol. 86, no. 10, pp. 3084–3098, Oct. 2012, doi: 10.1016/j.solener.2012.07.019.

[25] S. Kuravi, J. Trahan, Y. Goswami, C. Jotshi, E. Stefanakos, and N. Goel, 'Investigation of a High-Temperature Packed-Bed Sensible Heat Thermal Energy Storage System With Large-Sized Elements', *J. Sol. Energy Eng*, vol. 135, no. 041008, Jun. 2013, doi: 10.1115/1.4023969.

[26] '1414 Degrees | Clean Industrial Heat | 1414degrees.com.au'. Accessed: Nov. 05, 2025. [Online]. Available: https://1414degrees.com.au/

[27] 'Antora – Home', Antora. Accessed: Nov. 05, 2025. [Online]. Available: https://www.antora.com//

[28] 'Clean Energy Solutions for a Sustainable Future | Bren Energy'. Accessed: Nov. 05, 2025. [Online]. Available: https://bren-energy.com/

[29] 'Electrified Thermal Solutions – Electrifying industrial heat.' Accessed: Nov. 05, 2025. [Online]. Available: https://electrifiedthermal.com/

[30] 'Heatcube: Low-cost, net-zero heat. At scale. For Industry.' Accessed: Nov. 05, 2025. [Online]. Available: https://www.kyotogroup.no/

[31] 'Denmark - Countries & Regions', IEA. Accessed: Nov. 07, 2025. [Online]. Available: https://www.iea.org/countries/denmark

[32] E. Jakobsdottir, 'Annual Report 2024, Denmark', IEA Wind TCP. Accessed: Oct. 29, 2025. [Online]. Available: https://iea-wind.org/publications/danmark-annual-report-2024-publish/

[33] M. Cascetta, G. Cau, P. Puddu, and F. Serra, 'A comparison between CFD simulation and experimental investigation of a packed-bed thermal energy storage system', *Applied Thermal Engineering*, vol. 98, pp. 1263–1272, Apr. 2016, doi: 10.1016/j.applthermaleng.2016.01.019.

[34] S. Trevisan, B. Buchbjerg, and R. Guedez, 'Power-to-heat for the industrial sector: Techno-economic assessment of a molten salt-based solution', *Energy Conversion and Management*, vol. 272, p. 116362, Nov. 2022, doi: 10.1016/j.enconman.2022.116362.

[35] Y. Filali Baba, H. Ajdad, A. A. L. Mers, Y. Grosu, and A. Faik, 'Multilevel comparison between magnetite and quartzite as thermocline energy storage materials', *Applied Thermal Engineering*, vol. 149, pp. 1142–1153, Feb. 2019, doi: 10.1016/j.applthermaleng.2018.12.002.

[36] R. Tiskatine *et al.*, 'Suitability and characteristics of rocks for sensible heat storage in CSP plants', *Solar Energy Materials and Solar Cells*, vol. 169, pp. 245–257, Sep. 2017, doi: 10.1016/j.solmat.2017.05.033.

[37] B. Krüger, F. Dammel, and P. Stephan, 'Investigating the aspect ratio's influence on the exergetic performance and thermocline dynamics of a large water-based thermal energy storage system', *Journal of Energy Storage*, vol. 91, p. 112058, Jun. 2024, doi: 10.1016/j.est.2024.112058.

[38] M. Sadeghi, A. Chitsaz, S. M. S. Mahmoudi, and M. A. Rosen, 'Thermoeconomic optimization using an evolutionary algorithm of a trigeneration system driven by a solid oxide fuel cell', *Energy*, vol. 89, pp. 191–204, Sep. 2015, doi: 10.1016/j.energy.2015.07.067.

[39] F. G. Battisti, L. A. de Araujo Passos, and A. K. da Silva, 'Economic and environmental assessment of a CO2 solar-powered plant with packed-bed thermal energy storage', *Applied Energy*, vol. 314, p. 118913, May 2022, doi: 10.1016/j.apenergy.2022.118913.

[40] 'JRC Photovoltaic Geographical Information System (PVGIS) - European Commission'. Accessed: Dec. 15, 2025. [Online]. Available: https://re.jrc.ec.europa.eu/pvg_tools/en/

[41] 'National_Survey_Report_of_PV_Power_Applications_in_Denmark_-_2016.pdf'. Accessed: Dec. 15, 2025. [Online]. Available: https://iea-pvps.org/wp-content/uploads/2020/01/National_Survey_Report_of_PV_Power_Applications_in_Denmark_-_2016.pdf

[42] ‘Transparency Platform’. Accessed: Dec. 15, 2025. [Online]. Available: https://transparency.entsoe.eu/load/total/dayAhead?appState=%7B%22sa%22%3A%5B%22BZN%7C10Y1001A1001A46L%22%5D%2C%22st%22%3A%22BZN%22%2C%22mm%22%3Atrue%2C%22ma%22%3Afalse%2C%22sp%22%3A%22HALF%22%2C%22dt%22%3A%22CHART%22%2C%22df%22%3A%5B%222025-12-15%22%2C%222025-12-15%22%5D%2C%22tz%22%3A%22CET%22%7D

[43] J. Lago, G. Marcjasz, B. De Schutter, and R. Weron, ‘Forecasting day-ahead electricity prices: A review of state-of-the-art algorithms, best practices and an open-access benchmark’, *Applied Energy*, vol. 293, p. 116983, Jul. 2021, doi: 10.1016/j.apenergy.2021.116983.

[44] ‘European Wholesale Electricity Price Data’, Ember. Accessed: Aug. 13, 2025. [Online]. Available: https://ember-energy.org/data/european-wholesale-electricity-price-data

[45] ‘Natural gas prices’. Accessed: Dec. 16, 2025. [Online]. Available: https://www.kaggle.com/datasets/joebeachcapital/natural-gas-prices

[46] ‘Lifecycle cost analysis and performance evaluation of multi-stage screw compressors’. Accessed: Mar. 19, 2026. [Online]. Available: https://journals.sagepub.com/doi/epub/10.1177/09544062241312875